





Article

Antimicrobial Activity and DFT Studies of a Novel Set of Spiropyrrolidines Tethered with Thiochroman-4-one/Chroman-4-one Scaffolds

Nourhène Chouchène ¹, Amani Toumi ¹, Sarra Boudriga ^{1,*} , Hayet Edziri ², Mansour Sobeh ³ , Mohamed A. O. Abdelfattah ⁴, Moheddine Askri ¹, Michael Knorr ^{5,*} , Carsten Strohmann ⁶ , Lukas Brieger ⁶ and Armand Soldera ^{7,*}

¹ Laboratory of Heterocyclic Chemistry Natural Product and Reactivity (LR11ES39), Department of Chemistry, Faculty of Science of Monastir, University of Monastir, Monastir 5019, Tunisia; nourhene.chouchene23@gmail.com (N.C.); amanitoumi45@gmail.com (A.T.); moheddine.askri@fsm.rnu.tn (M.A.)

² Laboratoire des Maladies Transmissibles et des Substances Biologiquement Actives, Faculté de Pharmacie, Monastir 5000, Tunisia; jaziri_hayet@yahoo.fr

³ AgroBioSciences Research, Mohammed VI Polytechnic University, Lot 660–Hay MoulayRachid, Ben Guerir 43150, Morocco; mansour.sobeh@um6p.ma

⁴ College of Engineering and Technology, American University of the Middle East, Kuwait; Mohamed.AbdelMoety@aum.edu.kw

⁵ Institut UTINAM-UMR CNRS 6213, Université Bourgogne Franche-Comté, 16 Route de Gray, 25030 Besançon, France

⁶ Faculty of Chemistry, Inorganic Chemistry, Technical University Dortmund, Otto-Hahn-Strasse 6, 44227 Dortmund, Germany; carsten.strohmanna@tu-dortmund.de (C.S.); lukas.brieger@tu-dortmund.de (L.B.)

⁷ Laboratory of Physical Chemistry of Matter, Department of Chemistry, Université de Sherbrooke, Sherbrooke, QC J1K 2R1, Canada

* Correspondence: sarra.boudriga@fsm.rnu.tn (S.B.); michael.knorr@univ-fcomte.fr (M.K.); armand.soldera@usherbrooke.ca (A.S.)



Citation: Chouchène, N.; Toumi, A.; Boudriga, S.; Edziri, H.; Sobeh, M.; Abdelfattah, M.A.O.; Askri, M.; Knorr, M.; Strohmann, C.; Brieger, L.; et al. Antimicrobial Activity and DFT Studies of a Novel Set of Spiropyrrolidines Tethered with Thiochroman-4-one/Chroman-4-one Scaffolds. *Molecules* **2022**, *27*, 582. <https://doi.org/10.3390/molecules27030582>

Academic Editors:
Jean-Marc Sabatier,
Soumaya Kouidhi and
Athina Geronikaki

Received: 29 October 2021
Accepted: 20 December 2021
Published: 18 January 2022

Publisher's Note: MDPI stays neutral with regard to jurisdictional claims in published maps and institutional affiliations.



Copyright: © 2022 by the authors. Licensee MDPI, Basel, Switzerland. This article is an open access article distributed under the terms and conditions of the Creative Commons Attribution (CC BY) license (<https://creativecommons.org/licenses/by/4.0/>).

Abstract: A novel series of 14 spiropyrrolidines bearing thiochroman-4-one/chroman-4-one, and oxindole/acenaphthylene-1,2-dione moieties were synthesized and characterized by spectroscopic techniques, as well as by three X-ray diffraction studies, corroborating the stereochemistry. Quantum chemical calculations studies, using the DFT approach, were performed to rationalize the stereochemical outcome. These *N*-heterocycles were evaluated for their antibacterial and antifungal activities against some pathogenic organisms. Several compounds displayed moderate to excellent activity towards the screened microbe strains in the study compared to Amoxicillin (AMX), Ampicillin (AMP), and Amphotericin B. Furthermore, a structural activity relationship (SAR) was established considering the synthesized compounds. Pharmacokinetic studies reveal that these derivatives exhibit an acceptable predictive ADMET profile (Absorption, Distribution, Metabolism, Excretion and Toxicity) and good drug-likeness.

Keywords: [3+2] cycloaddition; thiochroman-4-one; chroman-4-one; spiropyrrolidine; crystal structure; DFT

1. Introduction

The emergence of drug-resistant pathogens has threatened human ability to treat common infections, and, thus, antimicrobial resistance (AMR) became a health threat all over the globe. The rapid spread of *Staphylococcus aureus*, for instance, is especially alarming, since it is considered to be among the most common causes of infections in health-care facilities [1,2]. Furthermore, patients suffering with infections caused by methicillin-resistant *Staphylococcus aureus* (MRSA) are more likely to die, compared to others infected with drug-sensitive infections, by about 64% [3,4]. Consequently, antimicrobial medications including antibiotics are getting more and more ineffective and, thus, infections become

difficult or nearly impossible to treat. This lowered efficacy urgently increases the demand for new therapeutic agents.

In recent years, spiro pyrrolidine scaffolds, especially those fused to oxindole or acenaphthylene-1(2*H*)-one moieties, and occurring in a huge number of pharmacological entities and natural compounds with significant bioactive properties, have attracted the attention of synthetic chemists [5–13] (Figure 1).

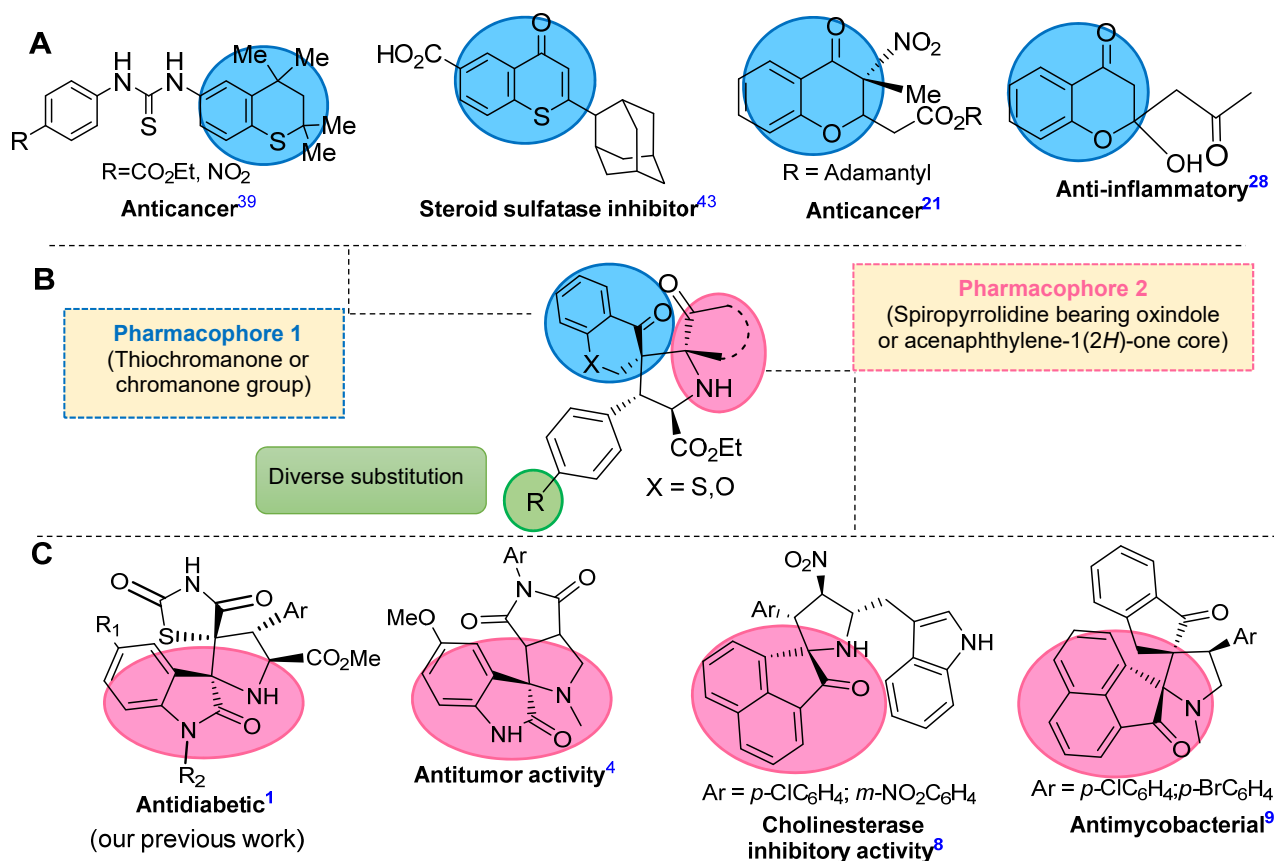


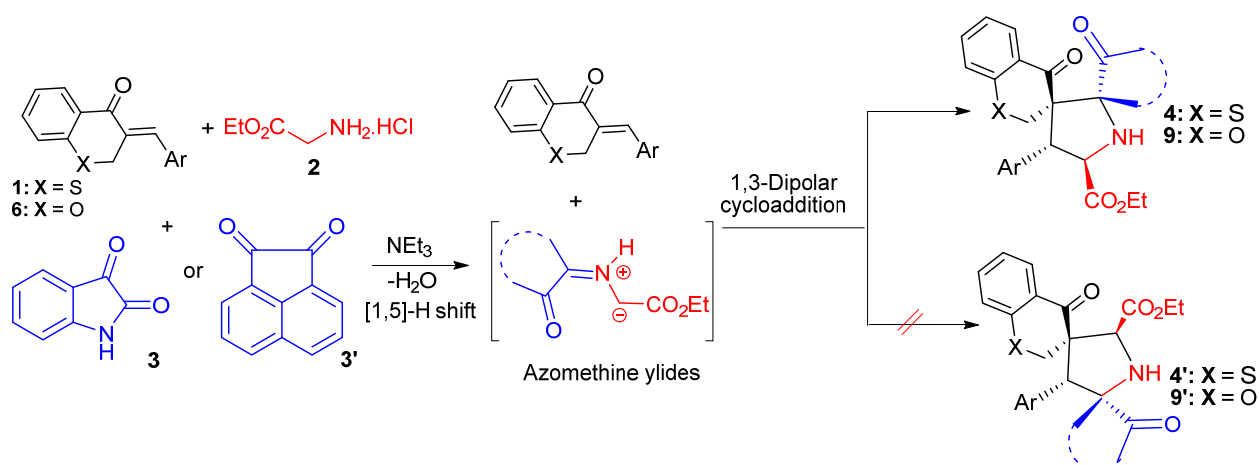
Figure 1. (A) Biologically relevant thiochroman, thiochromanone, and chromanone derivatives, (C) Biologically relevant spiro pyrrolidines bearing oxindole or acenaphthylene-1(2*H*)-one moieties, and (B) Our target compounds.

On the other hand, 4-chromanone derivatives represent privileged scaffolds in heterocyclic chemistry and for drug discovery. They are used as versatile intermediates for the synthesis of many natural products [14–19] and constitute interesting building blocks in drug design and organic synthesis [20–23]. They also exhibit significant biological activities allowing their use as anticancer [24–27], antifungal and antibacterial [28–31], anti-inflammatory [32,33], antidiabetic [34,35], anti-leishmanial (caused by protozoan parasites) [36,37], and insecticidal agents [38] (Figure 1).

Thiochromanones, the thio-analogs of chromanones, feature interesting scaffolds, which have been reported to exert a plethora of pronounced biological and pharmacological properties including antimicrobial [39–42], anticancer [43–46], human steroid sulfatase inhibition [47,48], α -adrenergic antagonist [49], antiviral [50], and insecticidal activities [51] (Figure 1).

In light of the significance of spiro pyrrolidine and thiochromanone/chromanone heterocycles in medicinal chemistry, we felt a great potential to combine these two moieties into one single scaffold to design a novel class of hybrid spiroheterocycles, which may exhibit interesting biological profiles. The latter were obtained via multicomponent reactions (MCRs) of arylidene thiochroman-4-ones/chroman-4-ones, glycine ethyl ester, and cyclic

1,2-diketones (isatin derivatives or acenaphthenequinone) (Scheme 1). We are aware that related spiropyrrolidine(s) fused with thiochroman-4-one/chroman-4-one moieties have been prepared by Subramaniyan [52] and Rani [53], however their pharmacological profile has, up to now, never been explored.



Scheme 1. Synthesis scheme for the target compounds 4 and 9.

In continuation of our research interests in the synthesis of novel bioactive *N*-spiroheterocycles [5,54–57], we herein report the synthesis of diverse thiochromanone/chromanone substituted spiropyrrolidines (Figure 1). The latter were obtained via multicomponent reactions (MCRs) of arylidene thiochroman-4-ones/chroman-4-ones, glycine ethyl ester, and cyclic 1,2-diketones (isatin derivatives or acenaphthenequinone) (Scheme 1). These new scaffolds were tested *in vitro* for their antimicrobial potential. DFT calculations were carried out to obtain the optimized molecular structures of the resulting spiranic thiochromanone/chromanone-linked spiropyrrolidines. Furthermore, frontiers molecular orbitals (FMO) and molecular electrostatic potential (MEP) calculations were performed for the structural exploration of these compounds. A drug-likeness analysis was also performed.

2. Results and Discussion

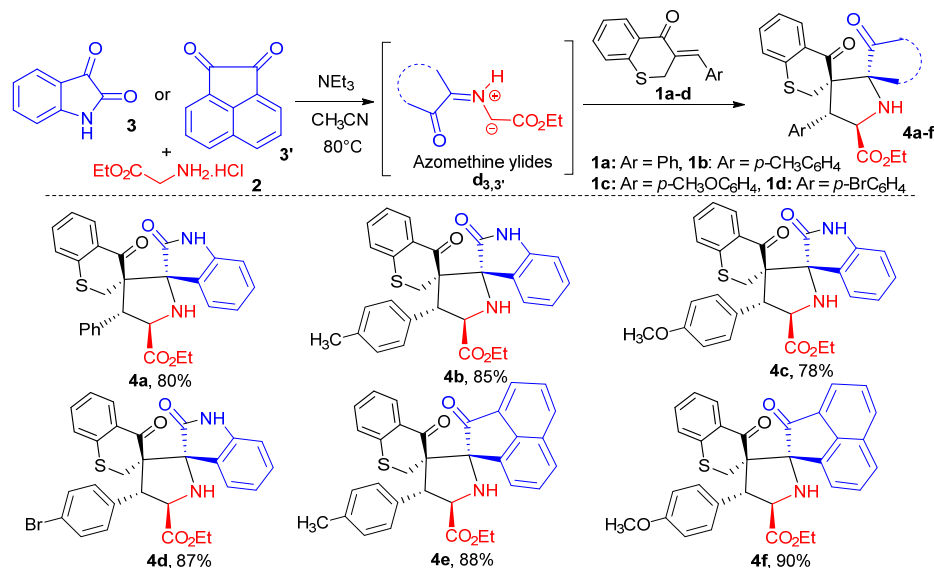
2.1. Synthetic Chemistry

The synthetic strategy for our target compounds 4 and 9 is shown in Scheme 1. It is based on a multicomponent process involving the 1,3-dipolar cycloaddition reaction between exocyclic arylated alkenes derived from thiochromanone 1 or chromanone 6 and azomethine ylides. The latter were generated *in situ* from condensation of glycine ethyl ester 2 and a 1,2-diketone, namely isatin 3 or acenaphthenequinone 3' (Scheme 1).

At the onset of our investigation, we attempted to access the hybrid thiochromanone-grafted spiropyrrolidines according to our recently established reaction conditions for MCR of arylidene rhodanines, glycine ethyl ester, and cyclic 1,2-diketones [5]. For that purpose, an equivalent amount of 3-benzylidene-thiochroman-4-one 1a, glycine ethyl ester 2, and isatin 3 was refluxed in acetonitrile in the presence of triethylamine for 2 h. The reaction smoothly afforded the desired spiroheterocycle 4a in 80% yield (Table 1). Subsequently, a variety of dipolarophiles 1 were subjected to these reaction conditions. As shown in Table 1, this process is applicable to a wider series of arylidene thiochromanones 1 bearing electronically different substituents, or groups, on the phenyl ring, affording in good yields the targeted spiropyrrolidine products 4b–d in a high regio- and diastereoselective manner as racemic mixtures. To expand the scope of this protocol, we further examined the multicomponent reaction with acenaphthenequinone 3' as an alternative 1,2-diketone, instead of isatin 3 (Table 1), to synthesize an original spiropyrrolidines scaffold bearing an acenaphthylen-1(2*H*)-one core. The azomethine ylide derived from acenaph-

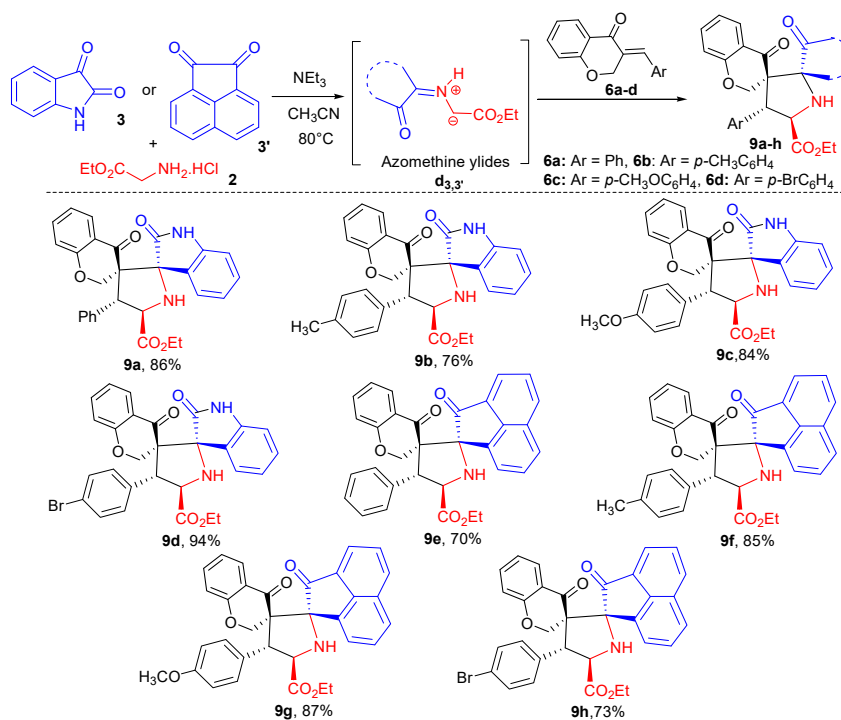
thenequinone seemed to be well appropriate for this process, affording the corresponding exo-spiropyrrolidine-chromanones **4e** and **4f** with good yields. Since this straightforward multicomponent [3+2] cycloaddition worked efficiently, we then studied the scope of the reaction using an oxygen surrogate, namely 5-arylidene chroman-4-ones **6**, under the same reaction conditions (Table 2).

Table 1. Synthesis of spiropyrrolidine-thiochroman-4-ones hybrids **4**.



All reactions were carried out using **1** (1 mmol), **2** (1 mmol), **3**, or **3'** (1 mmol), NEt_3 (1 mmol) in CH_3CN (5.0 mL) at reflux for 2 h. Yields of the isolated cycloadducts are given.

Table 2. Synthesis of acenaphthylen-1(2*H*)-one-spiropyrrolidine-chromanone hybrids **9**.



All reactions were carried out using **6** (1 mmol), **2** (1 mmol), **3**, or **3'** (1 mmol), NEt_3 (1 mmol) in CH_3CN (5.0 mL) at reflux for 2 h. Yields of the isolated cycloadducts are given.

The MCR proceeded readily providing the spiro pyrrolidines **exo-9a–h** as the only detectable diastereoisomers (TLC monitoring) with good to excellent yield (70–94%), regardless of the electronic nature of the *p*-substituent at the aryl group (H, OCH₃, CH₃, and Cl) of the dipolarophile **6**. On the other hand, the steric property of the acenaphthenequinone **3'** had almost a negligible effect on the efficiency of the 1,3-dipolar cycloaddition reaction, which proceeded smoothly producing the acenaphthylen-1(2*H*)-one spiro pyrrolidine-chromanones **9e–h** in excellent yields. All compounds are stable and were obtained as colorless or yellow solids.

2.1.1. Spectroscopic and Crystallographic Characterization of Cycloadducts **4** and **9**

The composition and stereochemistry of the chromanone/thiochromanone-grafted spiro pyrrolidines was unambiguously elucidated by their spectroscopic data and elemental analyses. The assignments of the chemical shifts from the ¹H and ¹³C NMR spectra of the studied compounds were done based on the literature data [5,53,55] and calculations at the B3LYP/6-311++G(2d,p) level of compounds **4a** and **9c** (Supplementary Materials; Table S1). As representative examples, relevant ¹H and ¹³C chemical shifts of spiro-compounds **4a** and **9c** are illustrated in Figures 2 and 3, respectively.

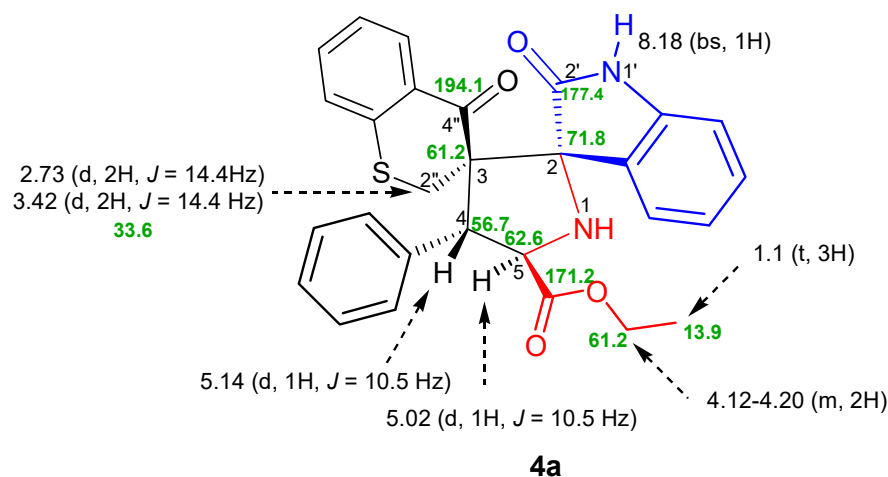


Figure 2. ¹H (black) and ¹³C (¹H) NMR (green) chemical shifts (ppm) of the selected compound **4a** (see also Figure S3 in the Supporting Material).

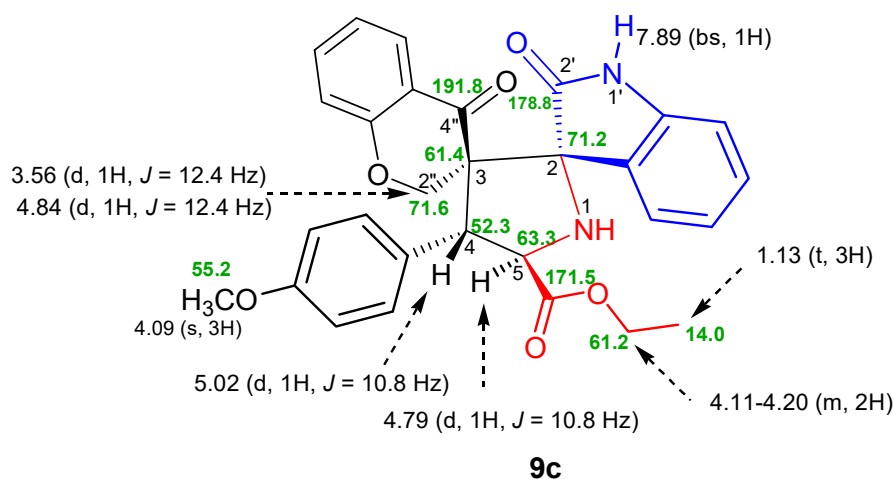


Figure 3. ¹H (black) and ¹³C (¹H) NMR (green) chemical shifts (ppm) of the selected compound **9c** (see also Figure S20 in the Supporting Material).

In the ^1H NMR spectra of **4a** and **9c**, the pyrrolidinyll protons H-4 and H-5 appear as two mutually coupled doublets at δ 5.14 and 5.02 ppm, and δ 5.02 and 4.79 ppm, respectively. This multiplicity unambiguously confirms the regiochemistry proposed in Figures 2 and 3. If the hypothetical alternative regioisomers **4'**, **9'** (Scheme 1) would have been formed, the pyrrolidinyll protons should give rise to two singlets in the ^1H NMR spectrum. Furthermore, the value of the 3J coupling constants of 10.5 and 10.8 Hz indicate that H-4 and H-5 protons are in *trans* relationship, in accordance with our earlier reports on related compounds [5,55]. A broadened singlet at δ 8.18 and 7.89 ppm can be assigned to the oxindole N-H proton of **4a** and **9c**, and a multiplet in the region between 6.59–8.17 ppm and 6.06–7.94 ppm indicates the presence of aromatic protons. Additionally, the ^1H NMR spectra show two mutually coupled doublets at δ 2.73 and 3.42 ppm for **4a**, and 3.56 and 4.84 ppm for **9c**, corresponding to the diastereotopic 2'- CH_2 group. The 3J values of 12.3 Hz for **4a** and 14.1 Hz for **9c** are in the same range with those previously reported values of similar spiropyrrolidine(s) fused with thiochroman-4-one/chroman-4-one moieties [52,53].

The proton decoupled ^{13}C NMR spectrum of **9c** reveals the presence of two signals at δ 191.8 and δ 178.8 ppm, attributed to the carbonyl groups of chromanone and oxindole moieties, respectively. The resonances corresponding to the two spirocarbons C-2 and C-3 are observed at δ 71.2 and δ 61.4 ppm, respectively. For the assignment of the methoxy, methylene, methine, spiro, and quaternary carbons, the DEPT-135 spectra shown in Figures S3 and S20 were recorded.

The relative configuration of the stereogenic carbons in spiropyrrolidines **4** and **9** was corroborated after determination of the single-crystal X-ray structures of cycloadducts **4a**, **4e**, and **9c**, whose molecular structures are shown in Figures 4–6, respectively. The structural analysis reveals that the carbonyl carbon of acenaphthenequinone moiety and (i) the carbonyl carbon group of thiochromanone/chromanone part are in *trans*-relationship, (ii) the pyrrolidinyll proton attached at C-5 (C-11, C-4, and C-18 in the crystal structures of **4a**, **4e**, and **9c**, respectively) are in *cis*-relationship (note that the crystallographic atom numbering scheme differs from that used in Figures 2 and 3).

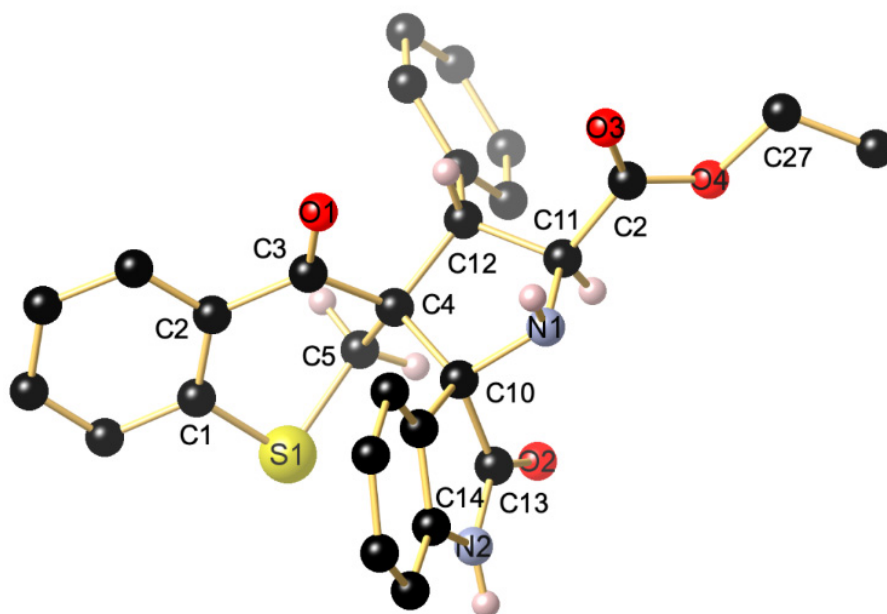


Figure 4. Ball and sticks presentation of the molecular structure of **4a** recorded at 100 K. Only one of the two independent molecules is shown. Apart from stereochemically relevant H atoms, all other hydrogen atoms are omitted for clarity. Furthermore, an EtOH molecule of crystallization, present in the asymmetric unit, is not depicted.

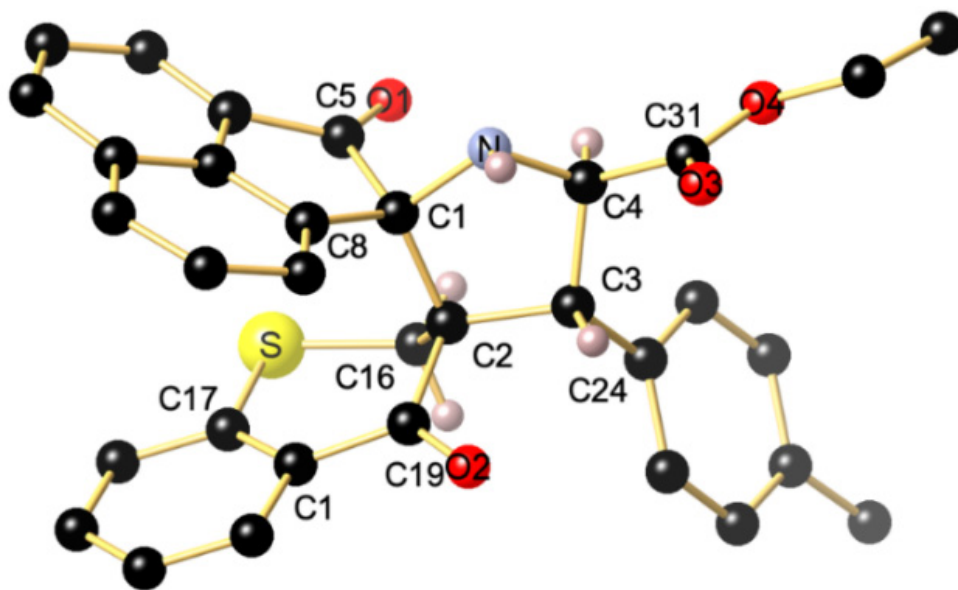


Figure 5. Ball and sticks presentation of the molecular structure of **4e** recorded at 100 K. Only stereochemically relevant H atoms are shown.

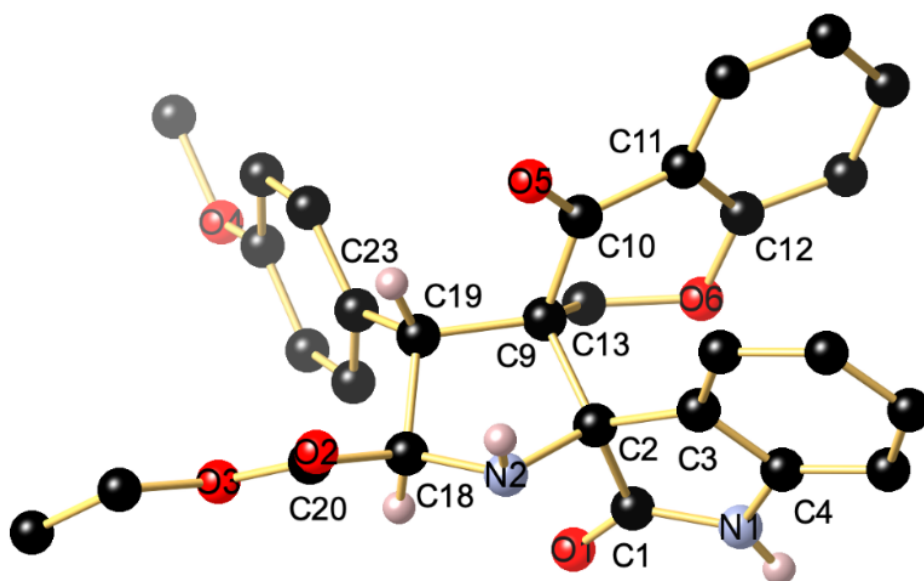


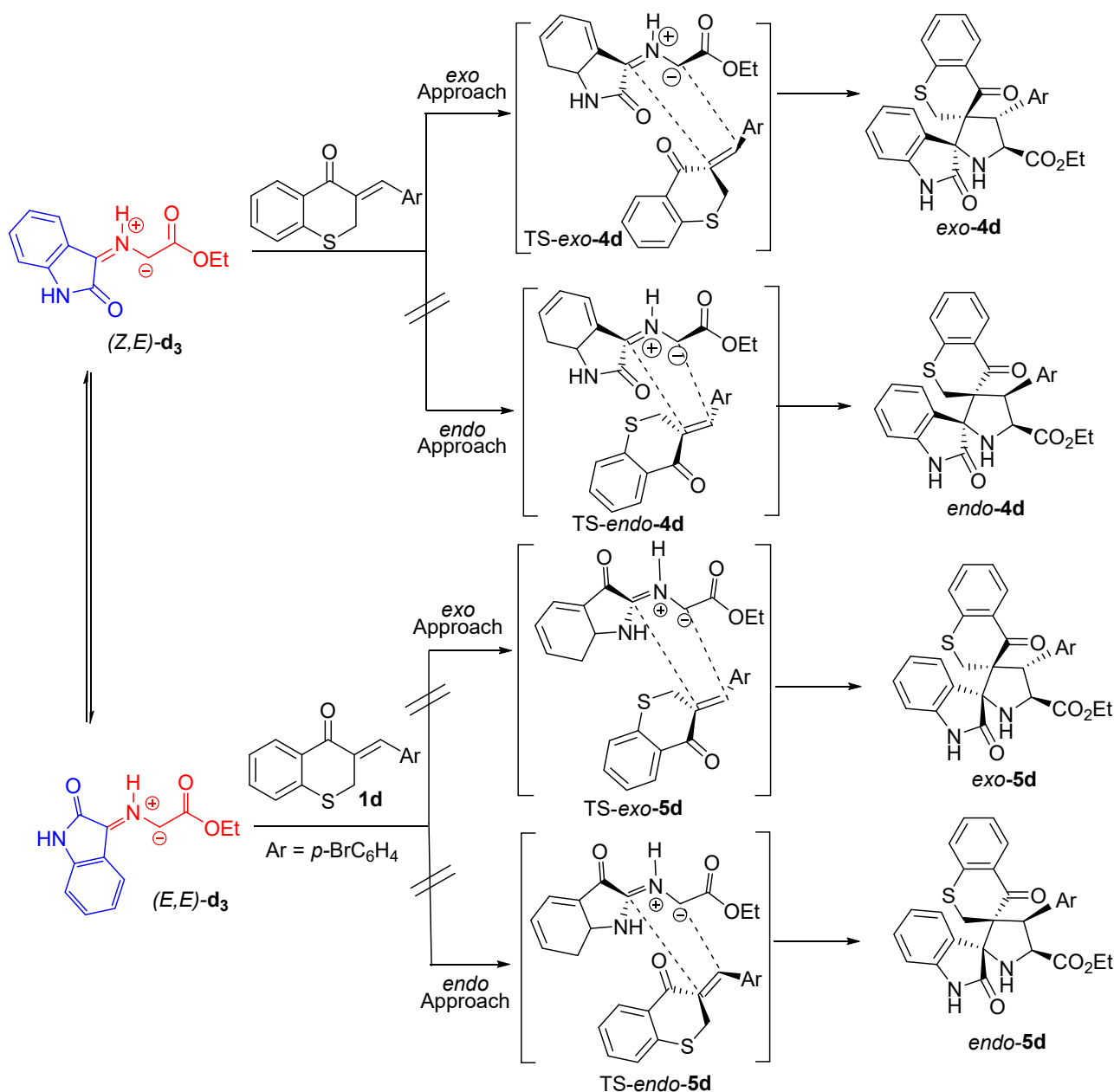
Figure 6. Ball and sticks presentation of the molecular structure of **9c** recorded at 100 K. Only one of the two independent molecules is shown. Apart from stereochemically relevant H atoms, all other hydrogen atoms are omitted for clarity.

It is noteworthy that the packing of **4a** contains two independent molecules with slightly different metric parameters, and the individual molecules are associated through intermolecular $N_2-H_2 \cdots O_6$ and $N_4-H_4 \cdots O_2$ hydrogen bonding with $H \cdots O$ bond lengths of 1.94 and 2.00 Å, respectively (see Figure S31). A similar supramolecular pairwise $N-H \cdots O$ association occurs also in the crystal structure of **9c** (see Figure S32).

Accordingly, we propose that the cycloadducts **4** and **9** are formed through an exo-approach between the arylidene thiochromanone/chromanone and the *Z,E*-dipole, as outlined above in Tables 1 and 2.

2.1.2. DFT Mechanistic Studies

To better grasp the experimentally observed high regio- and diastereoselectivity in the MCR, DFT calculations were performed using the 6-31G(d,p) basis set and the ω B97xd functional [58]. The effect of solvent (acetonitrile) was taken into consideration using the polarizable continuum model (PCM) approach [59,60]. We have chosen the reaction of dipolarophile **1a**, glycine ethyl ester **2**, and isatin **3** as model case study, as illustrated in Scheme 2.



Scheme 2. Proposed mechanism for the regio- and stereoisomeric 1,3-dipolar cycloaddition reaction of dipolarophile **1d** with azomethine ylide **d₃**.

In line with our previous study [55], condensation of a glycine ethyl ester and isatin, or acenaphthenequinone, followed by a [1,2]-prototropic sequence furnishes **(E,E)** and **(Z,E)** azomethine ylides are the two most stable isomers. Note that the subsequent 1,3-dipolar cycloaddition of these intermediates can a priori occur through both endo-TS and exo-

TSs (Scheme 2). Kinetic and thermodynamic calculations of the Gibbs free energy (ΔG), enthalpy (ΔH), and entropy (ΔS), corresponding to all possible isomeric pathways of the reaction and relative energies for the TSs, are summarized in Table 3.

Table 3. Difference in the Gibbs free energies (ΔG , in kcal mol⁻¹), enthalpies (ΔH , in kcal mol⁻¹), entropies (ΔS , in cal K⁻¹ mol⁻¹), and electronic energies (ΔU , in kcal mol⁻¹) for TSs and products calculated at the ω B97xd/6-31G(d,p) level of theory.

	ΔG	ΔH	ΔS	ΔU
TS- <i>exo-4d</i>	0.4	-17.6	-50.9	-16.9
TS- <i>endo-4d</i>	2.0	15.4	-48.9	-14.7
TS- <i>exo-5d</i>	15.1	-3.6	-52.7	-2.9
TS- <i>endo-5d</i>	14.9	-0.3	-42.7	0.4
<i>exo-4d</i>	-21.8	-42.4	-58.1	-41.7
<i>endo-4d</i>	-14.6	-34.8	57.0	-34.2
<i>exo-5d</i>	-16.8	-37.9	-59.5	-37.2
<i>endo-5d</i>	-16.3	-36.2	-56.3	-35.5

The analysis of the four located transition states reveals that TS-*exo-4d*, corresponding to the *exo*-approach between the (*E*)-*p*-bromobenzylidenethiochromanone **1d** and the (*Z,E*)-dipole, presents the lowest barriers with a ΔG value of 0.4 kcal mol⁻¹, favoring the formation of the observed *exo-4d* regioisomer. Moreover, ΔG values indicate that the product *exo-4d*, identified as the sole product is more stable (ΔG , -21.8 kcal mol⁻¹) than the other theoretical stereoisomers *endo-4d*, *exo-5d*, and *endo-5d*. Thus, the spiroadduct **4d** is kinetically and thermodynamically preferred, which agrees well with our experimental observations.

2.2. Biological Evaluation of the Synthesized Compounds

2.2.1. Antimicrobial Activity

The dispiropyrrolidine derivatives **4** and **9** were evaluated for their antibacterial activity against an assortment of five Gram-positive bacteria (*Bacillus subtilis* ATCC 6633, *Staphylococcus epidermidis* CI1232, *Staphylococcus aureus* ATCC 29213, *Staphylococcus aureus* ATCC 25923, and *Enterococcus faecalis* ATCC 29212) and four Gram-negative bacteria (*Escherichia coli* ATCC 25922, *Klebsiella pneumoniae* ATCC 4352, *Salmonella enterica* 800390, and *Pseudomonas aeruginosa* ATCC 9023). The antifungal activity of the synthesized compounds was also investigated against *Candida albicans* ATCC 90028, *Candida glabrata* ATCC 90030, and *Candida krusei* ATCC 6258. As references, to evaluate and to compare the potency of the tested compounds under the same conditions, the antibiotics Amoxicillin (AMX) and Ampicillin (AMP) were chosen as antibacterial agents. Macrocytic Amphotericin B was used as antifungal reference.

The in vitro antimicrobial activity of the novel dispiropyrrolidines has been assessed by the determination of the minimal inhibitory concentration (MIC) using the microdilution method, as described by Rattan [61]. The results are summarized in Tables 4 and 5.

Most of the screened compounds show variable antibacterial activities ranging from poor to excellent against Gram-positive and Gram-negative bacteria with MIC values in the range of 32–250 μ g/mL. As shown in Table 4, compounds **4a–e** exhibit, in most cases, interesting antibacterial potential. Compounds **4a–d** displayed the highest activity (MIC = 32 μ g/mL) towards *B. subtilis* and *S. epidermidis* compared to the reference antibiotics Amoxicillin (MIC = 64 μ g/mL) and Ampicillin (MIC = 78 μ g/mL).

Moreover, all these compounds were found to be more active than the standard drugs Amoxicillin (MIC = 64 μ g/mL) and Ampicillin (MIC = 78 μ g/mL) against the screened Gram-negative bacteria with MIC values ranging from 64 to 125 μ g/mL. For the series **9a–h**, results presented in Table 4 indicate that the most performant derivatives exhibit an inferior activity compared to the spirocompounds of series **4**. They show only a poor to moderate activity with MIC values ranging from 64 to 250 μ g/mL. It is noteworthy that

compounds **4a**, **4b**, **4d**, and **4e**, with MIC value of 64 µg/mL, perform with an excellent activity, up to four times higher towards *P. aeruginosa* than Amoxicillin (MIC = 256 µg/mL).

Table 4. MIC values (in µg/mL) of the target compounds **4** and **9** against Gram-positive and Gram-negative bacteria activities.

Comp.	Gram Positive Bacteria					Gram Negative Bacteria			
	<i>B. subtilis</i> ATCC 6633	<i>S. epidermidis</i> CI1232	<i>S. aureus</i> ATCC 29213	<i>S. aureus</i> ATCC 25923	<i>E. faecalis</i> ATCC 29212	<i>E. coli</i> ATCC 25922	<i>K. pneumo-</i> <i>niae</i> ATCC 4352	<i>S. enterica</i> 800390	<i>P. aeruginosa</i> ATCC 9023
4a	32	32	64	32	32	125	64	64	64
4b	32	32	64	32	32	125	64	64	125
4c	32	32	64	64	32	125	64	64	64
4d	32	32	64	64	32	125	64	64	64
4e	32	32	64	32	64	250	64	125	64
9a	125	250	125	125	125	250	250	550	250
9b	125	250	250	250	125	125	125	550	125
9c	125	125	125	250	64	250	64	550	125
9d	64	64	500	125	64	125	64	550	125
9e	125	250	125	125	64	250	64	550	125
9f	64	64	125	125	125	125	250	550	250
9g	64	64	125	125	125	125	500	500	500
9h	64	64	125	125	250	250	500	500	500
AMX ^a	64	-	-	-	1	256	256	-	256
AMP ^a	-	78	50	50	-	-	-	100	-

^a Positive control.

Table 5. Antifungal activity of synthesized compounds **4** and **9** (MIC was determined in µg/mL).

Compound	<i>Candida albicans</i> ATCC 90028	<i>Candida glabrata</i> ATCC 90030	<i>Candida krusei</i> ATCC 6258
4a	64	64	64
4b	64	64	64
4c	64	64	64
4d	64	32	32
4e	64	64	64
9a	250	250	250
9b	250	125	125
9c	125	125	125
9d	125	125	250
9e	500	500	500
9f	125	250	125
9g	250	125	250
9h	125	250	250
Amphotericin B ^a	500	500	500

^a Positive control.

The compounds **9d** and **9f–h** (MIC = 64 µg/mL) are more potent than Amoxicillin (MIC = 78 µg/mL) against *S. epidermidis* and exhibit an activity against *B. subtilis* similar to that of the reference antibiotic Ampicillin (MIC = 64 µg/mL). The results of antifungal screening (Table 5) reveal that compound **9e** was the only one exhibiting an activity comparable to that of reference antifungal Amphotericin B (MIC = 500 µg/mL) against the tested fungi.

The other synthesized compounds of series **4** were found to be more active than the standard drug with MICs ranging between 32–500 µg/mL. Notably, compound **4d** was found to be the most potent antifungal agent (MIC = 32 µg/mL) towards *C. krusei* and *C. glabrata* compared to the reference antifungal Amphotericin B (MIC = 500 µg/mL).

In contrast, compounds **9a–h** were revealed to be less active than their analogues, **4**, against the three screened yeasts with MIC values ranging from of 125–500 µg/mL.

2.2.2. Structure-Activity Relationship (SAR)

Another aim of these studies was to analyze qualitatively and quantitatively the structure-activity relationships (SAR) of our dispiropyrrolidines. As described in the literature, spiropyrrolidine derivatives are known to be excellent antimicrobial agents [8,62,63]. For the first screening of the in vivo antimicrobial results, it is clearly outlined that the presence of a thiochromanone moiety in spiropyrrolidines **4a–e**, independently of the nature of the *para*-substituent attached on the phenyl ring, greatly influences the inhibitory activity against all of the tested bacterial and fungal strains in comparison to their analogues containing a chromanone moiety **9a–h**. These results conclude the importance of the introduction of the thiochromanone moiety to improve the activity of spiropyrrolidines. Compounds **4a–e** especially feature a broad-spectrum bacterial and antifungal action and exerted the more potent antimicrobial effect as compared to the rest of the synthesized compounds.

Concerning the series **9a–d**, bearing an oxindole core, it is interesting to note that the introduction of an electron-withdrawing bromine substituent (**9d**) at the *para* position of the aromatic cycle of the chromanone, caused an increase of the antibacterial activity towards *B. subtilis*, *S. epidermis*, *E. coli*, *K. pneumoniae*, and *P. aeruginosa*. In contrast, the introduction of an electron-donating group, such as a methyl (**9b**) or methoxy group (**9c**), decreased the activity potency or retained it against the same bacteria.

Among the spiropyrrolidines incorporating an acenaphthylene-1(2*H*)-one core **9e–h**, compound **9e**, with an unsubstituted phenyl ring, is the most active one against *K. pneumoniae* and *P. aeruginosa*. Compounds **9f** (4-MePh), **9g** (4-MeOPh), and **9h** (4-BrPh) are found to exert a superior antibacterial effect against *B. subtilis* and *S. epidermis*. The inductive or mesomeric electronic effects exerted by these groups allow, probably, each bacterium to interact in its own specific way with the corresponding compounds.

According to the antifungal activity results and based on the study of the structure-activity relationships (SAR), we noticed that compounds containing a thiochromanone ring, **4a–e**, display significant antifungal activity against all the tested fungal strains, superior to those of the chromanone-grafted spiropyrrolidines, **9a–h**, and the reference antifungal Amphotericin B. In addition, the compound **4d** is the most potent one against *C. krusei* and *C. glabrata*. This finding shows that the presence of a bromine atom in *para* position of the phenyl group of chromanone seems to be responsible for the enhanced activity.

2.3. DFT Computational Studies

2.3.1. Optimized Molecular Structures and HOMO-LUMO Energies

The ground state geometric optimization of spiropyrrolidines **4a–f** and **9a–h** was carried out in the gas phase with the ω B97xd functional [58] and the standard 6–31g(d,p) basis set in Gaussian 16 package [64]. The simulated electron densities distribution of the FMOs, including both HOMO and LUMO orbitals of all compounds, are indicated in Table S2 (see Supporting Information). Frontier molecular orbital energies and chemical reactivity descriptor values of the optimized geometries are summarized in Tables 6 and 7.

Table 6. The HOMO, LUMO energies and molecular descriptors of compounds **4a–f**.

Compound	E_{HOMO}	E_{LUMO}	ΔE_{gap}	η	μ	ω
	(eV)					
4a	−7.463	−5.502	1.961	0.981	−6.483	21.422
4b	−7.462	−5.501	1.961	0.981	−6.482	21.415
4c	−7.459	−5.494	1.965	0.983	−6.477	21.338
4d	−7.462	−5.507	1.955	0.978	−6.485	21.501
4e	−7.497	−5.860	1.637	0.819	−6.679	27.234
4f	−7.496	−5.860	1.636	0.818	−6.678	27.259

Table 7. The HOMO, LUMO energies and molecular descriptors of compounds **9a–h**.

Compound	E_{HOMO}	E_{LUMO}	ΔE_{gap}	η	μ	ω
	(eV)					
9a	−8.386	−5.499	2.887	1.444	−6.943	16.692
9b	−8.387	−5.497	2.890	1.445	−6.942	16.675
9c	−8.380	−5.492	2.888	1.444	−6.936	16.658
9d	−8.387	−5.499	2.888	1.444	−6.943	16.692
9e	−8.449	−5.875	2.574	1.287	−7.162	19.928
9f	−8.447	−5.874	2.573	1.287	−7.161	19.922
9g	−8.426	−5.874	2.552	1.276	−7.150	20.032
9h	−8.448	−5.878	2.570	1.285	−7.163	19.964

The molecular frontier orbitals provide important clues to the chemical reactivity of molecules. The FMOs energy gap describes the charge transfer character from HOMO to LUMO within the studied compounds. The HOMO energy represents the tendency of a molecule to donate electrons, while the LUMO energy indicates the ability to accept electrons [65].

Thus, increasing the HOMO energy and decreasing the LUMO energy of the ligand lead to large intermolecular interactions with the LUMO and the HOMO of the receptor. The extent of these stabilizing interactions between ligand-receptor interacting orbitals correlates with the HOMO-LUMO energy gap. The softest molecules are determined with small energy gap values ($\Delta E_{\text{gap}} = E_{\text{LUMO}} - E_{\text{HOMO}}$) and are also identified as more stable and, hence, more reactive, according to Pearson's "Hard and Soft Acids and Bases" principle [66].

As shown from Table 4, the HOMO and LUMO electron-density of spiropyrrolidines **4a–f** is delocalized on the thiochromanone ring except in **4e** and **4f**, where the electron-density of the LUMO, which indicates the electrophilic attack site, is mainly distributed over the acenaphthene nucleus. For the designed compounds **9a–f**, the HOMO orbital was found to be distributed all over the pyrrolidine ring and isatin or acenaphthenequinone nucleus. However, the LUMO orbitals are dispersed over the chromanone ring in the series of compounds **9a–d** and on the acenaphthenequinone ring in compounds **9e–h**. Interestingly, the spiropyrrolidines **4a–f** bearing a thiochroman-4-one moiety show smaller energy gap values, ranging between 1.636 and 1.965 eV, compared to spiropyrrolidine derivatives **9a–h** featuring a chroman-4-one scaffold (ΔE_{gap} in the range of 2.552 and 2.890 eV). Consequently, compounds **4a–f** are the most reactive, compared to compounds **9a–h**, which show the lowest reactivity (the most chemically stable). These results may explain the higher biological activity of compounds **4a–f**, providing a good match with the experimental antifungal and antibacterial data.

The reactivity descriptors, based on the analysis of the electronic chemical potential (μ), the chemical hardness (η), and the electrophilicity index (ω), provide useful insight into the chemical reactivity and stability of the molecules. The chemical potential describes the electron transfer capacity that occurs in the molecule in the fundamental state and the propensity of electrons to escape from an equilibrium system, whereas the chemical hardness indicates the resistance to charge transfer [67,68]. As shown in Table 4, compounds **4a–f** showed higher chemical potential (ranging from −6.477 to −6.679 eV) and lower hardness values (in the range of 0.818 to 0.983 eV). Consequently, the spiropyrrolidines **4a–f** are softer and more reactive than the chromanone-grafted spiropyrrolidines **9a–h**. The biological activity of compounds **4a–f** can, thus, be affected by the strong charge transfer interaction. The electrophilicity (ω), which defines the tendency of molecules to attract electrons [69], is also superior in the series of spiropyrrolidines **4a–d**. Hence, the bioactivity of these compounds may be explained by the ability of the biological target to receive electrons from neighboring molecules, which may be important for stabilization of the active site.

2.3.2. Molecular Electrostatic Potential (MEP)

The MEP has emerged as a powerful approach in drug design and molecular biology to understand the intermolecular interactions between molecules and their biological receptors (proteins, enzymes). The MEP is applied to explore the chemical affinity and most likely binding modes with a molecular receptor, thus providing insight into the structure activity relationship of bioactive compounds. MEP-mapped surfaces inform on the chemical reactivity of the molecules and provide a reliable description of the charge distributions in a pictorial form. They also indicate the most likely electrophilic and nucleophilic reactive sites, polarization of molecules, as well as hydrogen bonding interactions [70–73].

The sites related to the polar and nonpolar regions of the molecule are visualized by color variations. Electrophilic regions are indicated by blue coloration (electron-deficient regions), while nucleophilic regions are shown in red color (electron-rich regions). The electrostatic potential maps of the selected compounds **4a**, **4e**, **9c**, **9d**, **9e**, and **9f** are shown in Figure 7.

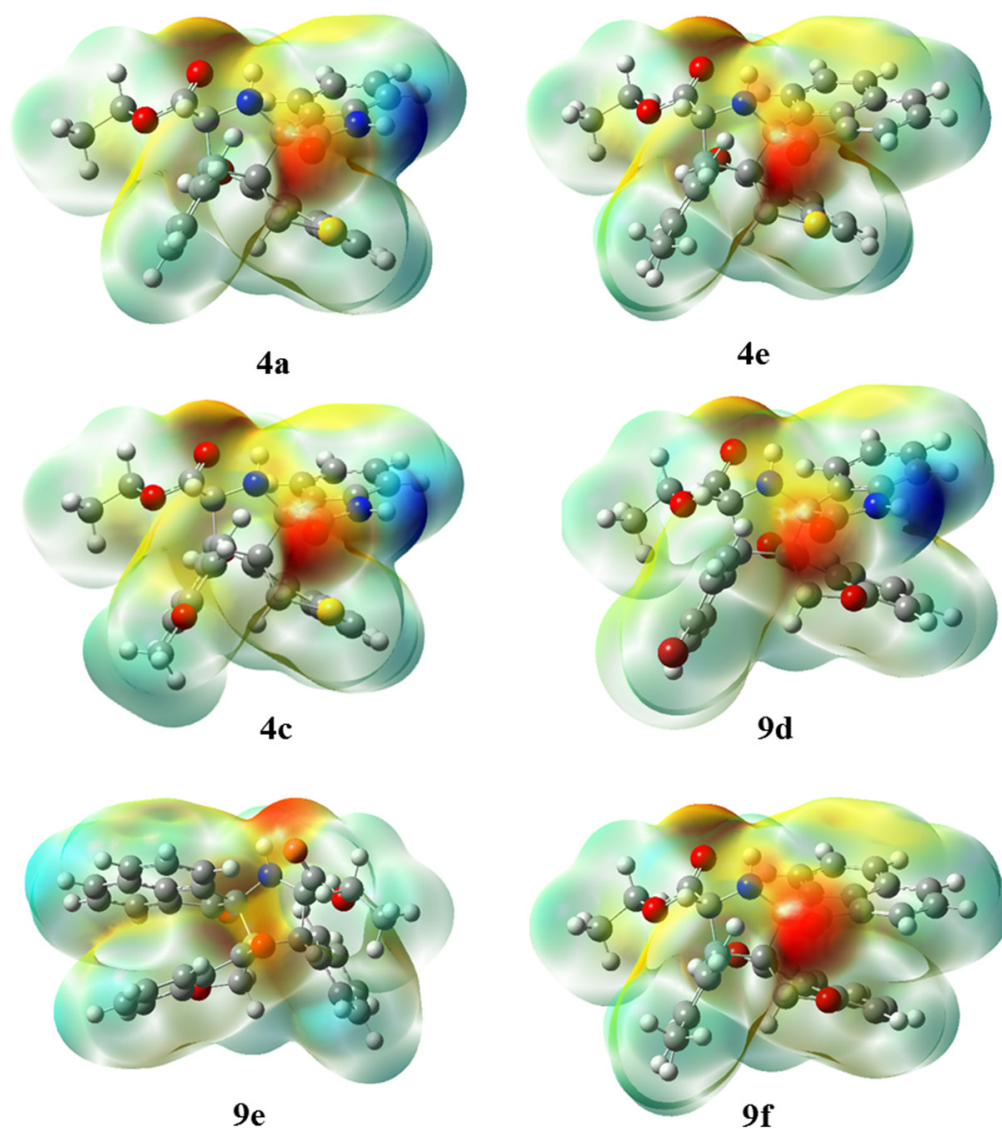


Figure 7. Molecular electrostatic potential (MEP) formed by mapping of the total density over the electrostatic potential for compounds **4a**, **4e**, **4c**, **9d**, **9e**, and **9f**.

2.4. Drug-Likeness Analysis

Analyzing the physicochemical properties of the developed drug hits is a crucial step to analyze and determine their drug-likeness potential. In this regard, quantitative structure-activity relationships (QSAR) descriptors, which can be calculated by means of a variety of software packages, may be a very useful tool. In this work, we evaluated the drug-likeness potential of the six selected compounds (**4a**, **4d**, **4e**, **9c**, **9d**, and **9e**) through computing various QSAR descriptors, according to the Lipinski rule of five [74] and the Veber's parameters (Table 8) [75].

Table 8. Results of Lipinski and Veber rules for the tested compounds.

Compound	4d	9d	9e	9c	4a	4e
lip_acc	6	7	6	8	6	5
lip_don	3	3	2	3	3	2
lip_druglike	1	1	1	1	1	0
lip_violation	1	1	1	0	0	2
logP(o/w)	4.46	3.83	4.81	2.99	3.67	5.75
Weight	564.48	548.41	504.56	499.54	485.58	534.66
TPSA	89.08	98.31	86.28	107.54	89.08	77.05
logS	−8.03	−7.06	−7.95	−6.02	−6.94	−9.4
vol	478.5	464.88	476	464.88	451.25	507.5
b_rotN	4	4	4	5	4	4
mr	14.37	13.8	14.32	13.68	13.61	15.34
a_hyd	27	26	29	26	26	31

Molecular weights of the compounds range from 485.58 to 564.48 Da. Derivatives **4a** and **9c**, having molecular weights less than 500 Da, obey the first Lipinski rule for effective and safe drug delivery. Lipinski's second rule stipulates that drug-like compounds should not possess more than five hydrogen bond donating groups. All of the six compounds comply with this rule. Hydrogen bond accepting groups in all compounds are in the range of 5–8, which is less than ten, thus also meeting Lipinski's third rule. The determined logP value was 2.99–5.75. All compounds, therefore, satisfy Lipinski's rule regarding logP with a value inferior to five. An exception is compound **4e**, whose logP value exceeds five. Compounds **4a** and **9c** showed zero Lipinski violations, compounds **4d**, **9d**, and **9e** violated one rule, while compound **4e** violated two rules and, thus, failed to show a drug-likeness potential (Table 8). Veber's parameters, such as molar refractivity (mr) and total polar surface area (TPSA), demonstrate the polarizability of the compounds and suggest their oral bioavailability [75]. The mr values of the six compounds did not fall in the recommended range of 40–130 cm³/mol, however, this was offset by their TPSA value, which was not superior to 140 for any of the compounds. This suggests, for derivatives, an appreciable oral bioavailability. Besides, the number of rotatable bonds is four or five, which is inferior to 10. Except for compound **4e**, which failed in drug-likeness parameters, some additional parameters, such as solubility, van der Waals volume, and number of hydrophobic atoms (a-hyd) were found to be in the acceptable range of −6 to −8, 451–478, and 26–31, respectively.

3. Materials and Methods

3.1. Apparatus and General Information

The ¹H NMR spectra were recorded at 300 and 400 MHz using a Bruker Avance 300 or Bruker Avance III-400 machine (Rheinstetten, Germany). The chemical shifts were recorded in ppm relative to TMS and with the solvent resonance as the internal standard. Data were reported as follows: chemical shift, multiplicity (bs = broad singlet, s = singlet, d = doublet, t = triplet, m = multiplet), coupling constants (Hz), integration. ¹³C {¹H} NMR data were collected at 75 or 100 MHz with complete proton decoupling with the solvent resonance as the internal standard. Elemental analyses were performed on a Perkin Elmer 2400 Series II

Elemental CHNS analyzer (Waltham, MA, USA). Materials: thin-layer chromatography (TLC): TLC plates (Merck, silica gel 60 F254 0.2 mm, 200 × 200 nm) (Darmstadt, Germany); substances were detected using UV light at 254 nm.

3.2. General Procedure for Preparation of Cycloadducts 4 and 9

A mixture of 3-arylideneethiochroman-4-ones/3-arylidenechroman-4-ones (1 mmol), ethyl glycinate hydrochloride (1 mmol) **2**, isatin **3** or acenaphthenequinone **3'** (1 mmol), and Et₃N (1 mmol) in acetonitrile (5 mL) was heated under reflux for 2h. After completion of the reaction (TLC monitoring), the solvent was removed under vacuum. The residue was chromatographed on silica gel employing ethylacetate-cyclohexane (3:7 v/v) as eluent to obtain the pure products **4** and **9**.

3.2.1. (2S*,3R*,4*S,5S*)-Spiro[2,3']-oxindole-spiro[3,3'']thiochroman-4''-one-4-phenyl-5-carboxyethoxypyrrolidine (**4a**)

White solid; Yield: (387 mg, 80%); mp (°C ± 2) = 184 °C; IR (KBr) ν : 3267, 2918, 1723, 1692, 1650, 1183, 749 cm⁻¹; ¹H NMR (300 MHz, CDCl₃) δ_{H} : 1.10 (t, $J = 7.2$ Hz, 3H, CH₃(ester)), 2.73 (d, $J = 14.4$ Hz, 1H, H-2''), 3.42 (d, $J = 14.4$ Hz, 1H, H-2''), 4.12–4.2 (m, 2H, CH₂(ester)), 5.02 (d, $J = 10.5$ Hz, 1H, H-4), 5.14 (d, $J = 10.5$ Hz, 1H, H-5), 6.59–6.62 (m, 1H, Ar-H), 6.72–6.74 (m, 1H, Ar-H), 6.81–6.84 (m, 1H, Ar-H), 6.97–7.05 (m, 2H, Ar-H), 7.09–7.12 (m, 2H, Ar-H), 7.28–7.40 (m, 3H, Ar-H), 7.56–7.58 (m, 1H, Ar-H), 8.14–8.17 (m, 1H, Ar-H), 8.18 (bs, 1H, H-1'); ¹³C NMR (75 MHz, CDCl₃) δ_{C} : 13.9, 33.6, 56.7, 61.2, 61.7, 62.6, 71.8, 110.0, 122.0, 124.7, 125.6, 126.0, 126.6, 127.6, 128.5, 126.6, 130.1, 130.7, 132.6, 136.2, 141.4, 142.2, 171.2, 177.4, 194.1. Anal. Calcd for C₂₈H₂₄N₂O₄S: C, 69.40; H, 4.99; N, 5.78%. Found: C, 69.07; H, 4.95; N, 5.79%.

3.2.2. (2S*,3R*,4*S,5S*)-Spiro[2,3']-oxindole-spiro[3,3'']thiochroman-4''-one-4-(p-methyl phenyl)-5-carboxyethoxypyrrolidine (**4b**)

White solid; Yield: (423 mg, 85%); mp (°C ± 2) = 218 °C; IR (KBr) ν : 3323, 2969, 1714, 1700, 1658, 1195, 759 cm⁻¹; ¹H NMR (300 MHz, CDCl₃) δ_{H} : 1.13 (t, $J = 6.9$ Hz, 3H, CH₃(ester)), 2.69 (s, 3H, CH₃), 2.74 (d, $J = 14.1$ Hz, 1H, H-2''), 3.39 (d, $J = 14.4$ Hz, 1H, H-2''), 4.11–4.19 (m, 2H, CH₂(ester)), 4.95 (d, $J = 10.2$ Hz, 1H, H-4), 5.05 (d, $J = 10.5$ Hz, 1H, H-5), 6.55–6.60 (m, 1H, Ar-H), 6.68–6.81 (m, 3H, Ar-H), 6.89–7.32 (m, 4H, Ar-H), 7.41–7.43 (m, 2H, Ar-H), 8.09–8.14 (m, 2H, Ar-H); ¹³C NMR (75 MHz, CDCl₃) δ_{C} : 13.5, 21.0, 32.2, 54.6, 55.4, 60.6, 61.9, 63.1, 72.0, 109.5, 113.1, 121.5, 124.6, 126.6, 129.0, 129.4, 131.3, 132.0, 132.3, 141.5, 141.6, 158.4, 178.1, 192.4. Anal. Calcd for C₂₉H₂₆N₂O₄S: C, 69.86; H, 5.26; N, 5.62%. Found: C, 69.53; H, 5.30; N, 5.63%.

3.2.3. (2S*,3R*,4*S,5S*)-[2,3']-oxindole-spiro[3,3'']thiochroman-4''-one-4-(p-methoxyphenyl)-5-carboxyethoxypyrrolidine (**4c**)

White solid; Yield: (401 mg, 78%); mp (°C ± 2) = 168 °C; IR (KBr) ν : 3270, 2925, 1734, 1697, 1655, 1194, 764 cm⁻¹; ¹H NMR (300 MHz, CDCl₃) δ_{H} : 1.12 (t, $J = 7.2$ Hz, 3H, CH₃(ester)), 2.53 (d, $J = 14.1$ Hz, 1H, H-2''), 3.39 (d, $J = 14.1$ Hz, 1H, H-2''), 3.80 (s, 3H, OCH₃), 4.12–4.19 (m, 2H, CH₂(ester)), 4.93 (d, $J = 10.5$ Hz, 1H, H-4), 4.99 (d, $J = 10.5$ Hz, 1H, H-5), 6.57–6.72 (m, 2H, Ar-H), 6.80–6.90 (m, 4H, Ar-H), 6.96–7.10 (m, 3H, Ar-H), 7.46–7.48 (m, 2H, Ar-H), 8.13–8.15 (m, 1H, Ar-H), 8.22 (bs, 1H, H-1'); ¹³C NMR (75 MHz, CDCl₃) δ_{C} : 13.5, 33.2, 54.6, 56.0, 60.5, 61.4, 62.6, 71.5, 109.2, 113.4, 121.4, 124.1, 125.4, 125.9, 126.0, 128.0, 128.8, 130.1, 130.3, 130.6, 131.9, 140.8, 141.7, 158.4, 171.3, 177.8, 193.8. Anal. Calcd for C₂₉H₂₆N₂O₄S: C, 67.69; H, 5.09; N, 5.44%. Found: C, 67.36; H, 5.13; N, 5.45%.

3.2.4. (2S*,3R*,4*S,5S*)-[2,3']-oxindole-spiro[3,3'']thiochroman-4''-one-4-(p-bromophenyl)-5-carboxyethoxypyrrolidine (**4d**)

White solid; Yield: (490 mg, 87%); mp (°C ± 2) = 221 °C; IR (KBr) ν : 3277, 2922, 1744, 1708, 1660, 1178, 754 cm⁻¹; ¹H NMR (300 MHz, CDCl₃) δ_{H} : 1.12 (t, $J = 7.2$ Hz, 3H, CH₃(ester)), 2.70 (d, $J = 14.4$ Hz, 1H, H-2''), 3.32 (d, 1H, $J = 14.4$ Hz, 1H, H-2''), 4.13–4.21 (m, 2H, CH₂(ester)), 4.93 (d, $J = 10.2$ Hz, 1H, H-4), 5.11 (d, $J = 10.5$ Hz, 1H, H-5), 6.53–6.58 (m,

1H, Ar-H), 6.74–6.92 (m, 3H, Ar-H), 6.96–7.15(m, 3H, Ar-H), 7.49–7.59 (m, 4H, Ar-H), 8.13–8.14 (m, 1H, Ar-H), 8.16 (bs, 1H, H-1'); ¹³C NMR (75 MHz, CDCl₃) δ_C: 14.0, 33.5, 55.5, 61.0, 61.7, 62.4, 71.7, 110.4, 121.9, 122.1, 124.3, 125.0, 126.8, 130.0, 130.5, 130.7, 131.8, 131.9, 133.0, 135.0, 141.9, 142.3, 170.4, 176.3, 194.2. Anal. Calcd for C₂₈H₂₃BrN₂O₄S: C, 59.69; H, 4.11; N, 4.97%. Found: C, 59.58; H, 4.26; N, 5.01%.

3.2.5. (2*S**,3*R**,4*S*,5*S**)-Spiro[2,2']-acenaphthene-1'-one-spiro[3,3']thiochroman-4''-one-4-(*p*-methylphenyl)-5-carboxyethoxypyrrolidine (**4e**)

White solid; Yield: (469 mg, 88%); mp (°C ± 2) = 128 °C; IR (KBr) ν: 3291, 3054, 1724, 1709, 1661, 1188, 783, 749 cm⁻¹; ¹H NMR (300 MHz, CDCl₃) δ_H: 1.11 (t, *J* = 7.2 Hz, 3H, CH₃(ester)), 2.35 (s, 3H, CH₃), 2.70 (d, *J* = 14.1 Hz, 1H, H-2''), 3.30 (d, *J* = 14.4 Hz, 1H, H-2''), 4.13–4.19 (m, 2H, CH₂(ester)), 5.13 (s, 2H, H-4 and H-5), 6.49–6.52 (m, 1H, Ar-H), 6.94–6.98 (m, 2H, Ar-H), 7.15–7.27 (m, 4H, Ar-H), 7.46–7.48 (m, 2H, Ar-H), 7.59–7.61 (m, 1H, Ar-H), 7.66–7.71 (m, 1H, Ar-H), 7.39–7.99 (m, 2H, Ar-H), 8.05–8.08 (m, 1H, Ar-H); ¹³C NMR (75 MHz, CDCl₃) δ_C: 14.0, 21.0, 33.5, 56.3, 61.3, 62.7, 63.1, 74.7, 122.2, 122.7, 124.7, 125.6, 126.6, 127.6, 128.1, 129.3, 129.7, 130.3, 130.5, 130.9, 131.3, 131.9, 132.4, 132.7, 135.6, 137.3, 141.7, 171.3, 194.0, 201.8. Anal. Calcd for C₃₃H₂₇NO₄S: C, 74.28; H, 5.10; N, 2.62%. Found: C, 74.06; H, 5.14; N, 2.60%.

3.2.6. (2*S**,3*R**,4*S*,5*S**)-Spiro[2,2']-acenaphthene-1'-one-spiro[3,3']thiochroman-4''-one-4-(*p*-methoxyphenyl)-5-arboxyethoxypyrrolidine (**4f**)

White solid; Yield: (494 mg, 90%); mp (°C ± 2) = 114 °C; IR (KBr) ν: 3282, 2990, 1718, 1705, 1662, 1186, 779, 736 cm⁻¹; ¹H NMR (300 MHz, CDCl₃) δ_H: 1.09 (t, *J* = 7.2 Hz, 3H, CH₃(ester)), 2.68 (d, *J* = 14.4 Hz, 1H, H-2''), 3.30 (d, *J* = 14.4 Hz, 1H, H-2''), 3.79 (s, 3H, OCH₃), 4.1–4.16 (m, 2H, CH₂(ester)), 5.01 (d, *J* = 10.8 Hz, 1H, H-4), 5.11 (d, *J* = 10.8 Hz, 1H, H-5), 6.47–6.48 (m, 1H, Ar-H), 6.87–6.94 (m, 3H, Ar-H), 7.12–7.26 (m, 2H, Ar-H), 7.48–7.56 (m, 3H, Ar-H), 7.62–7.72 (m, 2H, Ar-H), 7.88–7.94 (m, 2H, Ar-H), 8.02–8.05 (m, 1H, Ar-H); ¹³C NMR (75 MHz, CDCl₃) δ_C: 14.0, 33.5, 55.0, 56.3, 61.3, 62.7, 63.1, 74.7, 122.2, 122.7, 124.7, 125.6, 126.6, 127.6, 128.1, 129.3, 129.7, 130.3, 130.5, 130.9, 131.3, 131.9, 132.4, 132.7, 135.6, 136.0, 137.3, 171.3, 194.0, 201.8. Anal. Calcd for C₃₃H₂₇NO₅S: C, 72.11; H, 4.95; N, 2.55%. Found: C, 72.44; H, 4.99; N, 2.57%.

3.2.7. (2*S**,3*R**,4*S*,5*S**)-Spiro[2,3']-oxindole-spiro[3,3']chroman-4''-one-4-phenyl-5-carboxyethoxypyrrolidine (**9a**)

White solid; Yield: (402 mg, 86%) mp (°C ± 2) = 182 °C; IR (KBr) ν: 3331, 2974, 1726, 1701, 1682, 759 cm⁻¹; ¹H NMR (300 MHz, CDCl₃) δ_H: 1.00 (t, *J* = 7.2 Hz, 3H, CH₃(ester)), 3.46 (d, *J* = 12.3 Hz, 1H, H-2''), 4.01–4.10 (m, 2H, CH₂(ester)), 4.72 (d, *J* = 10.5 Hz, 1H, H-4); 4.75 (d, *J* = 12.3 Hz, 1H, H-2''), 4.98 (d, *J* = 10.5 Hz, 1H, H-5), 6.47–6.50 (m, 1H, Ar-H), 6.72–6.78 (m, 2H, Ar-H), 6.92–6.98 (m, 2H, Ar-H), 7.13–7.15 (m, 1H, Ar-H), 7.23–7.30 (m, 3H, Ar-H), 7.49–7.52 (m, 2H, Ar-H), 7.61–7.64 (m, 1H, Ar-H), 8.17 (bs, 1H, H-1'); ¹³C NMR (75 MHz, CDCl₃) δ_C: 13.9, 53.0, 61.1, 61.6, 63.1, 71.3, 71.5, 109.3, 116.7, 120.8, 121.1, 122.2, 125.8, 126.6, 127.7, 128.5, 129.3, 129.5, 134.9, 135.3, 140.8, 161.1, 171.6, 179.2, 191.7. Anal. Calcd for C₂₈H₂₄N₂O₅: C, 71.78; H, 5.16; N, 5.98%. Found: C, 71.60; H, 5.06; N, 5.89%.

3.2.8. (2*S**,3*R**,4*S*,5*S**)-Spiro[2,3']-oxindole-spiro[3,3']chroman-4''-one-4-(*p*-methylphenyl)-5-carboxyethoxypyrrolidine (**9b**)

Yellow solid; Yield: (366 mg, 76%); mp (°C ± 2) = 226 °C; IR (KBr) ν: 3281, 3002, 1716, 1695, 1675, 764 cm⁻¹; ¹H NMR (400 MHz, CDCl₃) δ_H: 1.10 (t, *J* = 7.1 Hz, 3H, CH₃(ester)), 2.30 (s, 3H, CH₃), 3.54 (d, *J* = 12.4 Hz, 1H, H-2''), 4.10–4.16 (m, 2H, CH₂(ester)), 4.78 (d, *J* = 10.8 Hz, 1H, H-4), 4.84 (d, *J* = 12.4 Hz, 1H, H-2''), 5.02 (d, *J* = 10.8 Hz, 1H, H-5), 6.59 (d, *J* = 8.1 Hz, 2H, Ar-H), 6.80–6.69 (m, 2H, Ar-H), 7.02–6.92 (m, 2H, Ar-H), 7.21–7.10 (m, 3H, Ar-H), 7.39 (d, *J* = 7.8 Hz, 2H, Ar-H), 7.62 (dd, *J* = 7.9 Hz, *J* = 1.5 Hz, 1H, Ar-H), 8.36 (bs, 1H, H-1'); ¹³C NMR (100 MHz, CDCl₃) δ_C: 14.0, 21.1, 52.7, 61.2, 61.5, 63.2, 71.3, 71.5, 109.3, 116.7, 121.1, 122.2, 125.8, 127.7, 129.2, 129.5, 131.7, 135.4, 137.3, 161.1, 171.7, 179.3, 191.8. Anal. Calcd for C₂₉H₂₆N₂O₅: C, 71.78; H, 5.16; N, 5.98%. Found: C, 71.60; H, 5.06; N, 5.89%.

3.2.9. (2*S,3*R**,4*S*,5*S**)-Spiro[2,3']-oxindole-spiro[3,3'']chroman-4''-one-4-(*p*-methoxyphenyl)-5-carboxyethoxypyrrolidine (9c)**

Yellow solid; Yield: (418 mg, 84%); mp ($^{\circ}\text{C} \pm 2$) = 228 $^{\circ}\text{C}$; IR (KBr) ν : 3315, 2985, 1721, 1688, 1674, 748 cm^{-1} ; ^1H NMR (300 MHz, CDCl_3) δ_{H} : 1.13 (t, $J = 7.1$ Hz, 3H, $\text{CH}_3(\text{ester})$), 3.51 (d, $J = 12.3$ Hz, 1H, H-2''), 3.81 (s, 3H, OCH_3), 4.13–4.19 (m, 2H, $\text{CH}_2(\text{ester})$), 4.76 (d, $J = 12.3$ Hz, 1H, H-2''), 4.91 (d, $J = 11.1$ Hz, 1H, H-4), 5.09 (d, $J = 11.1$ Hz, 1H, H-5), 6.00 (d, $J = 8.3$ Hz, 1H, Ar-H), 6.53 (t, $J = 7.5$ Hz, 1H, Ar-H), 6.94–6.71 (m, 3H, Ar-H), 7.36 (ddd, $J = 33.3$ Hz, $J = 18.9$ Hz, $J = 7.7$ Hz, 4H, Ar-H), 7.52 (d, $J = 8.1$ Hz, 1H, Ar-H), 7.60 (t, $J = 7.6$ Hz, 1H, Ar-H), 7.83 (d, $J = 8.1$ Hz, 1H, Ar-H), 7.91 (d, $J = 7.0$ Hz, 1H, Ar-H); ^{13}C NMR (75 MHz, CDCl_3) δ_{C} : 14.0, 52.3, 55.2, 61.2, 61.4, 63.3, 71.2, 71.6, 109.2; 113.9, 116.7, 120.8, 121.1, 122.2, 125.8, 126.4, 126.7, 127.7, 129.5, 135.3, 140.6, 159.0, 161.1, 171.5, 178.8, 191.8. Anal. Calcd for $\text{C}_{29}\text{H}_{26}\text{N}_2\text{O}_6$: C, 69.87; H, 5.26; N, 5.62%. Found: C, 69.00; H, 5.37; N, 5.59%.

3.2.10. (2*S,3*R**,4*S*,5*S**)-Spiro[2,3']-oxindole-spiro[3,3'']chroman-4''-one-4-(*p*-bromophenyl)-5-carboxyethoxypyrrolidine (9d)**

White solid; Yield: (514 mg, 94%); mp ($^{\circ}\text{C} \pm 2$) = 234 $^{\circ}\text{C}$; IR (KBr) ν : 3323, 2969, 1714, 1694, 1696, 749 cm^{-1} ; ^1H NMR (400 MHz, CDCl_3) δ_{H} : 1.11 (t, $J = 7.1$ Hz, 3H, $\text{CH}_3(\text{ester})$), 3.53 (d, $J = 12.3$ Hz, 1H, H-2''), 4.10–4.18 (m, 2H, $\text{CH}_2(\text{ester})$), 4.77 (t, $J = 10.7$ Hz, 2H, H-4 and H-2''), 5.00 (d, $J = 10.6$ Hz, 1H, H-5), 6.62–6.50 (m, 2H, Ar-H), 6.72 (dt, $J = 28.4$ Hz, $J = 7.6$ Hz, 2H, Ar-H), 6.98–6.86 (m, 2H, Ar-H), 7.21–7.10 (m, 1H, Ar-H), 7.42 (m, 4H, Ar-H), 7.62 (dd, $J = 7.9$ Hz, $J = 1.4$ Hz, 1H, Ar-H); 8.22 (bs, 1H, H-1'); ^{13}C NMR (100 MHz, CDCl_3) δ_{C} : 14.0, 52.3, 61.3, 63.2, 71.4, 71.5, 109.4, 116.7, 120.7, 121.3, 121.7, 125.8, 127.8, 129.6, 131.1, 131.7, 134.2, 135.6, 140.7, 161.1, 171.4, 191.7. Anal. Calcd for $\text{C}_{28}\text{H}_{23}\text{BrN}_2\text{O}_5$: C, 61.44; H, 4.24; N, 5.12%. Found: C, 61.58; H, 4.16; N, 5.20%.

3.2.11. (2*S,3*R**,4*S*,5*S**)-Spiro[2,2']-acenaphthene-1'-one-spiro[3,3'']chroman-4''-one-4-phenyl-5-carboxyethoxypyrrolidine (9e)**

Yellow solid; (352 mg, 70%); mp ($^{\circ}\text{C} \pm 2$) = 188 $^{\circ}\text{C}$; IR (KBr) ν : 3279, 2911, 1726, 1693, 1674, 1193, 774, 760 cm^{-1} ; ^1H NMR (400 MHz, CDCl_3) δ_{H} : 1.10 (t, $J = 7.1$ Hz, 3H, $\text{CH}_3(\text{ester})$), 3.47 (d, $J = 12.3$ Hz, 1H, H-2''), 4.13–4.18 (m, 2H, $\text{CH}_2(\text{ester})$), 4.75 (d, $J = 12.3$ Hz, 1H, H-2''), 4.90 (d, $J = 11.2$ Hz, 1H, H-4), 5.10 (d, $J = 11.1$ Hz, 1H, H-5), 6.01 (d, $J = 7.9$ Hz, 1H, Ar-H), 6.64–6.45 (m, 1H, Ar-H), 6.83 (m, 1H, Ar-H), 7.15 (d, $J = 7.8$ Hz, 2H, Ar-H), 7.47–7.20 (m, 5H, Ar-H), 7.55 (m, 2H, Ar-H), 7.85 (d, $J = 8.0$ Hz, 1H, Ar-H), 7.93 (d, $J = 6.9$ Hz, 1H, Ar-H); ^{13}C NMR (100 MHz, CDCl_3) δ_{C} : 14.0, 52.2, 61.2, 62.9, 63.2, 71.0, 74.6, 116.1, 120.7, 120.8, 121.5, 122.2, 125.1, 127.2, 127.9, 128.9, 129.2, 129.8, 131.0, 131.5, 131.7, 134.7, 136.9, 137.3, 140.8, 160.0, 171.9, 191.6. Anal. Calcd for $\text{C}_{32}\text{H}_{25}\text{NO}_5$: C, 76.33; H, 5.00; N, 2.78%. Found: C, 76.99; H, 5.06; N, 2.70%.

3.2.12. (2*S,3*R**,4*S*,5*S**)-Spiro[2,2']-acenaphthene-1'-one-spiro[3,3'']chroman-4''-one-4-(*p*-methylphenyl)-5-carboxyethoxypyrrolidine (9f)**

Yellow solid; Yield: (377 mg, 73%); mp ($^{\circ}\text{C} \pm 2$) = 194 $^{\circ}\text{C}$; IR (KBr) ν : 3288, 2898, 1739, 1700, 1667, 1201, 786, 767 cm^{-1} ; ^1H NMR (400 MHz, CDCl_3) δ_{H} : 1.10 (t, $J = 7.1$ Hz, 3H, $\text{CH}_3(\text{ester})$), 2.30 (s, 3H, CH_3), 3.47 (d, $J = 12.3$ Hz, 1H, H-2''), 4.10–4.17 (m, 2H, $\text{CH}_2(\text{ester})$), 4.75 (d, $J = 12.3$ Hz, 1H, H-2''), 4.90 (d, $J = 11.2$ Hz, 1H, H-4), 5.10 (d, $J = 11.1$ Hz, 1H, H-5); 6.01 (d, $J = 7.9$ Hz, 1H, Ar-H), 6.64–6.45 (m, 1H, Ar-H), 6.83 (m, 1H, Ar-H), 7.15 (d, $J = 7.8$ Hz, 2H, Ar-H), 7.47–7.20 (m, 5H, Ar-H), 7.55 (m, 2H, Ar-H), 7.85 (d, $J = 8.0$ Hz, 1H, Ar-H), 7.93 (d, $J = 6.9$ Hz, 1H, Ar-H); ^{13}C NMR (100 MHz, CDCl_3) δ_{C} : 14.0, 21.0, 52.7, 61.2, 63.2, 71.3, 71.5, 109.3, 116.7, 120.1, 122.2, 125.8, 126.6, 127.7, 129.2, 129.5, 131.7, 135.7, 140.8, 161.1, 171.7, 179.3, 191.8. Anal. Calcd for $\text{C}_{33}\text{H}_{27}\text{NO}_5$: C, 76.58; H, 5.26; N, 2.71%. Found: C, 76.49; H, 5.38; N, 2.76%.

3.2.13. (2S*,3R*,4*S,5S*)-Spiro[2,2']-acenaphthene-1'-one-spiro[3,3'']chroman-4''-one-4-(p-methoxyphenyl)-5-carboxyethoxypyrrolidine (**9g**)

Yellow solid; Yield: (464 mg, 87%); mp ($^{\circ}\text{C} \pm 2$) = 184 $^{\circ}\text{C}$; IR (KBr) ν : 3292, 2899, 1737, 1704, 1677, 1199, 773, 747 cm^{-1} ; ^1H NMR (400 MHz, CDCl_3) δ_{H} : 1.10 (t, $J = 7.1$ Hz, 3H, CH_3 (ester)), 3.55 (d, $J = 12.4$ Hz, 1H, H-2''), 3.77 (s, 3H, OCH_3), 4.10–4.16 (m, 2H, CH_2 (ester)), 4.76 (d, $J = 10.8$ Hz, 1H, H-4), 4.83 (d, $J = 12.3$ Hz, 1H, H-2''), 4.98 (d, $J = 10.8$ Hz, 1H, H-5), 6.59 (d, $J = 8.0$ Hz, 2H, Ar-H), 6.74 (dt, $J = 15.3$ Hz, $J = 7.6$ Hz, 2H, Ar-H), 6.87 (d, $J = 8.5$ Hz, 2H, Ar-H), 6.94 (m, 2H, Ar-H), 7.17 (t, $J = 7.3$ Hz, 1H, Ar-H), 7.43 (d, $J = 8.3$ Hz, 2H, Ar-H), 7.62 (m, 1H, Ar-H); ^{13}C NMR (100 MHz, CDCl_3) δ_{C} : 14.0, 52.4, 55.2, 61.2, 61.5, 63.4, 71.4, 71.6, 109.3, 113.9, 116.7, 120.8, 121.1, 122.2, 125.8, 126.6, 126.8, 127.7, 129.4, 130.4, 135.4, 140.8, 159.0, 161.1, 171.1, 171.8, 191.9. Anal. Calcd for $\text{C}_{33}\text{H}_{27}\text{NO}_6$: C, 74.28; H, 5.10; N, 2.63%. Found: C, 71.35; H, 5.17; N, 2.53%.

3.2.14. (2S*,3R*,4*S,5S*)-Spiro[2,2']-acenaphthene-1'-one-spiro[3,3'']chroman-4''-one-4-(p-bromophenyl)-5-carboxyethoxypyrrolidine (**9h**)

Yellow solid; Yield: (425 mg, 73%); mp ($^{\circ}\text{C} \pm 2$) = 226 $^{\circ}\text{C}$; IR (KBr) ν : 3285, 2883, 1752, 1713, 1687, 1192, 792, 773 cm^{-1} ; ^1H NMR (400 MHz, CDCl_3) δ_{H} : 1.11 (t, $J = 7.1$ Hz, 3H, CH_3 (ester)), 3.45 (d, $J = 12.2$ Hz, 1H, H-2''), 4.12–4.17 (m, 2H, CH_2 (ester)); 4.70 (d, $J = 12.2$ Hz, 1H, H-2''), 4.88 (d, $J = 11.1$ Hz, 1H, H-4), 5.08 (d, $J = 11.1$ Hz, 1H, H-5), 6.01 (d, $J = 8.3$ Hz, 1H, Ar-H), 6.85 (s, 1H, Ar-H), 6.57 (s, 1H, Ar-H), 7.29 (d, $J = 6.8$ Hz, 1H, Ar-H), 7.38–7.33 (m, 1H, Ar-H), 7.41 (m, 3H, Ar-H), 7.49 (d, $J = 8.4$ Hz, 2H, Ar-H), 7.54 (d, $J = 8.2$ Hz, 1H, Ar-H), 7.66–7.59 (m, 1H, Ar-H), 7.89 (m, 2H, Ar-H); ^{13}C NMR (75 MHz, CDCl_3) δ_{C} : 14.0, 51.8, 61.3, 63.2, 70.9, 74.6, 116.1, 121.0, 121.7, 122.2, 125.2, 127.2, 127.9, 128.0, 130.8, 131.1, 131.7, 134.9, 160.0, 171.5, 191.4, 204.4. Anal. Calcd for $\text{C}_{32}\text{H}_{24}\text{BrNO}_5$: C, 65.99; H, 4.15; N, 2.40%. Found: C, 65.90; H, 4.20; N, 2.55%.

3.3. Crystal Structure Determinations

X-ray suitable crystals were grown in EtOH. The crystal structure determination was accomplished on a Bruker D8 Venture four-circle diffractometer using a PHOTON 100 CMOS (**4a**, **9c**), or PHOTON II CPAD (**4e**), detector by Bruker AXS GmbH. X-ray radiation was generated by microfocus source $I\mu\text{S-Mo}$ ($\lambda = 0.71073$ Å) by Incoatec GmbH with HELIOS mirror optics and a single-hole collimator by Bruker AXS GmbH. The crystals of **4a**, **4e**, and **9c** were covered with an inert oil (perfluoropolyalkylether) and mounted on a MicroMount from MiTeGen. For the data collection, the programs APEX 3 Suite (v.2018.7-2), with the integrated programs SAINT (integration) and SADABS (adsorption correction) by Bruker AXS GmbH, were used. The processing and finalization of the crystal structures was done with the program Olex2 [76]. The crystal structure was solved with the ShelXT [77] structure solution program using Intrinsic Phasing and refined with the ShelXL [78] refinement package using Least Squares minimization. The non-hydrogen atoms were refined anisotropically. The C-bound and H atoms were placed in geometrically calculated positions and each was assigned a fixed isotropic displacement parameter based on a riding-model: C–H = 0.95–0.99 Å with $U_{\text{iso}}(\text{H}) = 1.5U_{\text{eq}}(\text{CH}_3)$ and $1.2U_{\text{eq}}(\text{CH}_2, \text{CH})$ for other hydrogen atoms. The N-bound hydrogen atoms were located in the difference-Fourier-map and refined independently. The crystal and structure refinement data of **4a**, **4e**, and **9c** are gathered in Table S3. Crystallographic data for the structures of **4a**, **4e**, and **9c** have been deposited with the Cambridge Crystallographic Data Centre as supplementary publication number 2116000 (**4a**), 2116001 (**4e**), and 2115999 (**9c**). Copies of these data can be obtained, free of charge, on application to CCDC, 12 Union Road, Cambridge, CB2 1EZ, UK; fax: 144-(0)1223-336033 or e-mail: deposit@ccdc.cam.ac.uk.

3.4. Antimicrobial Activity

3.4.1. Determination of the Antibacterial and Antifungal Activity

Various concentrations of the screened compounds have been used to determine their antimicrobial activity. Both cultures have been set to yield approximately 1×10^6 CFU mL $^{-1}$ of bacteria or yeast overnight. The minimum inhibitory concentrations (MICs) have been

determined on brain heart infusion (BHI) agar plates (Bio-Rad, Marne la Coquette, France) by a standard method (Edziri et al., 2012). One milliliter of each of the extracts, previously dissolved in 10% dimethyl sulfoxide (DMSO), have been mixed for each concentration with 19 mL of BHI agar at 40 °C and poured over Petri dishes. The resulting DMSO concentration was approximately 0.5%. Plates containing only medium, or medium with 0.5% DMSO, were used as controls to ensure that DMSO did not affect the growth. Standard antibiotics Amoxicillin (AMX) and Ampicillin (AMP), and the antifungal Amphotericin B were used to control the sensitivity of the tested microorganism. After 18 h of incubation at 37 °C, the MIC was defined as the lowest concentration of the extract inhibiting the visible growth of each microorganism. Each test was carried out in triplicate.

3.4.2. Microorganisms

The antibacterial potential of the dispiropyrrolidine derivatives has been investigated against nine microorganisms, namely the Gram-positive *Staphylococcus epidermidis* (C11232), *Bacillus subtilis* (ATCC 6633), *Staphylococcus aureus* (ATCC 29213), *Staphylococcus aureus* (ATCC 25923), and *Enterococcus faecalis* (ATCC 29212) and the Gram-negative rods *Escherichia coli* (ATCC 25922), *Klebsiella pneumoniae* (ATCC 4352), *Salmonella enterica* 800390, and *Pseudomonas aeruginosa* (ATCC 9023). For the evaluation of the antifungal activity, *Candida glabrata* (ATCC 90030), *Candida albicans* (ATCC 90028), and *Candida krusei* (ATCC 6258) have been used. As references, to evaluate and to compare the potency of the tested compounds under the same conditions, the antibiotics Amoxicillin (AMX) and Ampicillin (AMP) were chosen as antibacterial agents. Macrocytic Amphotericin B was used as antifungal reference (both of the previously identified bacterial and fungal strains were obtained from the laboratory of Transmissible Diseases and Biologically Active Substances, Faculty of Pharmacy, Tunisia).

3.5. Computational Methods

DFT calculations were performed using the Gaussian 16 suite of programs [64]. All geometry optimizations and frequency analyses were carried out using the ω B97xd functional with the standard 6-31G(d,p) basis set [58]. Vibrational analyses were performed to identify the stationary points as either local minima, or transition states (with one imaginary vibrational mode) on the potential energy surface. Solvent effects were considered using the polarizable continuum model (PCM) with acetonitrile as the solvent medium at a temperature of 355 K [59,60]. The frontier molecular orbitals analysis (FMOs) and molecular electrostatic potential (MEP) surfaces for compounds **4a–f** and **9a–h** were calculated at the same level of theory and visualized with the graphical interface Gauss View 6 [79] (Gaussian Inc., Wallingford, CT, USA). The chemical reactivity descriptors [80–82] (electronic chemical potential (μ), electronegativity (χ), chemical hardness (η), and electrophilicity index (ω) are calculated as follows: $\mu = (E_H + E_L)/2$; $\eta = (E_L - E_H)/2$; $\omega = (\mu^2/2\eta)$.

4. Conclusions

A *one-pot* three-component 1,3-dipolar cycloaddition reaction of a stabilized azomethine ylide, generated in situ by thermal [1,2]-prototropy of the corresponding iminoesters with (*E*)-3-arylidene-thiochroman-4-one/chroman-4-one as dipolarophiles afforded the dispiro-oxindole-pyrrolidine-thiochroman-4-ones, **4a–f** and dispiro-oxindole-pyrrolidine-chroman-4-ones, **9a–h** in satisfactory yields along with high regio- and stereoselectivity. DFT calculations correctly predicted the observed experimental results, evidencing that the reaction is favorable according to kinetic and thermodynamic parameters. The antimicrobial activity of the novel *N*-heterocyclic compounds was examined against different pathogenic bacteria and fungi. According to the antimicrobial activity results, and on the basis of a structure-activity relationships (SAR) study, it follows that compounds **4a–d** containing a thiochromanone ring display a significant antimicrobial activity against most of the tested bacterial and fungal strains, superior than those of chromanone-grafted spiropyrrrolidines **9a–h**. Even the activity of reference antibiotics is outperformed in some cases. Theoretical

chemical reactivity, taking into account the FMOs and MEP maps, predicted a relatively higher chemical reactivity and softer character of spiropyrrolidines **4a–f**, which seems to have a prominent effect on their higher antimicrobial activity compared to the **9a–h** derivatives. The predicted absorption, distribution, metabolism, and excretion (ADME) profiles of some derivatives were in line with Lipinski rules. These promising results encourage further study of the antimicrobial activity of these derivatives by measuring their toxicity. Advanced docking studies are in progress and will be published elsewhere.

Supplementary Materials: The following are available online, copies of ^1H and ^{13}C $\{^1\text{H}\}$ NMR spectra of compounds **4** and **9**, figures of the supramolecular interactions occurring in the crystalline states for **4a** and **9c**, DFT and Cartesian coordinates and energies.

Author Contributions: Supervision, methodology, analyses of obtained results, S.B., M.K., A.T., M.A. and A.S.; methodology, analyses of obtained results, writing the manuscript, S.B., M.K., A.T. and A.S.; synthesis, N.C.; X-ray diffraction analysis, M.K., C.S. and L.B.; antimicrobial assays, H.E.; drug-likeness analysis, M.S. and M.A.O.A.; DFT study, A.T. and A.S. All authors have read and agreed to the published version of the manuscript.

Funding: This work was supported by the LR11ES39 Grant from the Ministry of Higher Education and Scientific Research, Tunisia.

Institutional Review Board Statement: Not applicable.

Informed Consent Statement: Not applicable.

Data Availability Statement: The data presented in this study are not available from the authors.

Acknowledgments: The authors are grateful to the Ministry of Higher Education and Scientific Research of Tunisia for financial support (LR11ES39). Computations from the Calcul Quebec and Compute Canada are gratefully acknowledged. M.K. and C.S. acknowledge funding from the CNRS and the Deutsche Forschungsgemeinschaft. The authors would like to thank R. Rashied for her help in collecting the docking data.

Conflicts of Interest: The authors declare no conflict of interest.

Sample Availability: Samples of the compounds are available from the authors.

References

1. Tong, S.Y.C.; Davis, J.S.; Eichenberger, E.; Holland, T.L.; Fowler, V.G., Jr. *Staphylococcus aureus* Infections: Epidemiology, Pathophysiology, Clinical Manifestations, and Management. *Clin. Microbiol. Rev.* **2015**, *28*, 603–661. [[CrossRef](#)] [[PubMed](#)]
2. Lowy, F.D. Antimicrobial resistance: The example of *Staphylococcus aureus*. *J. Clin. Investig.* **2003**, *111*, 1265–1273. [[CrossRef](#)]
3. WHO. Antimicrobial Resistance. 2018. Available online: www.who.int/news-room/fact-sheets/detail/antimicrobial-resistance (accessed on 30 April 2014).
4. Gurung, R.R.; Maharjan, P.; Chhetri, G.G. Antibiotic resistance pattern of *Staphylococcus aureus* with reference to MRSA isolates from pediatric patients. *Future Sci. OA* **2020**, *6*, FSO464. [[CrossRef](#)] [[PubMed](#)]
5. Toumi, A.; Boudriga, S.; Hamden, K.; Sobeh, M.; Cheurfa, M.; Askri, M.; Knorr, M.; Strohmman, B.C.L. Synthesis, antidiabetic activity and molecular docking study of rhodanine-substituted spirooxindole pyrrolidine derivatives as novel α -amylase inhibitors. *Bioorg. Chem.* **2021**, *106*, 104507. [[CrossRef](#)]
6. Kumar, R.S.; Almansour, A.I.; Arumugam, N.; Mohammad, F.; Kumar, R.R. In vitro Mechanistic Exploration of Novel Spiropyrrolidine Heterocyclic Hybrids as Anticancer Agents. *Front. Chem.* **2020**, *20*, 465. [[CrossRef](#)] [[PubMed](#)]
7. Singh, G.S.; Desta, Z.Y. Isatins as Privileged Molecules in Design and Synthesis of Spiro-Fused Cyclic Frameworks. *Chem. Rev.* **2012**, *112*, 6104–6155. [[CrossRef](#)]
8. Arun, Y.; Bhaskar, G.; Balachandran, C.; Ignacimuthu, S.; Perumal, P.T. Facile One-Pot Synthesis of Novel Dispirooxindole-Pyrrolidine Derivatives and Their Antimicrobial and Anticancer Activity Against A549 Human Lung Adenocarcinoma Cancer Cell Line. *Bioorg. Med. Chem. Lett.* **2013**, *23*, 1839–1845. [[CrossRef](#)] [[PubMed](#)]
9. Jossang, A.; Jossang, P.; Hadi, H.A.; Sevenet, T.; Bodo, B. Horsfieldine, an oxindole alkaloid from *Horsfieldia superba*. *J. Org. Chem.* **1991**, *56*, 6527–6530. [[CrossRef](#)]
10. Kelemen, Á.A.; Satala, G.; Bojarski, A.J.; Keserú, G.M. Spiro[pyrrolidine-3,3'-oxindoles] and Their Indoline Analogues as New 5-HT₆ Receptor Chemotypes. *Molecules* **2017**, *22*, 2221. [[CrossRef](#)]
11. Boudriga, S.; Haddad, S.; Murugaiyah, V.; Askri, M.; Knorr, M.; Strohmman, C.; Golz, C. Three-Component Access to Functionalized Spiropyrrolidine Heterocyclic Scaffolds and Their Cholinesterase Inhibitory Activity. *Molecules* **2020**, *25*, 1963. [[CrossRef](#)]

12. Arumugama, N.; Almansoura, A.I.; Kumara, R.S.; Altafa, M.; Padmanabanc, R.; Sureshbabuc, P.; Angamuthuc, G.; Kotreshad, D.; Manohare, T.S.; Venketeshe, S. Spiropyrrolidine/spiroindolizino[6,7-b]indole heterocyclic hybrids: Stereoselective Synthesis, Cholinesterase Inhibitory Activity and Their Molecular Docking Study. *Bioorg. Chem.* **2018**, *79*, 64–71. [[CrossRef](#)]
13. Wei, A.C.; Ali, M.A.; Yoon, Y.K.; Ismail, R.; Choon, T.S.; Kumar, R.S. A Facile Three-Component [3+2]-Cycloaddition for the Regioselective Synthesis of Highly Functionalised Dispiropyrrolidines Acting as Antimycobacterial Agents. *Bioorg. Med. Chem. Lett.* **2013**, *23*, 1383–1386. [[CrossRef](#)] [[PubMed](#)]
14. Chenera, B.; West, M.L.; Finkelstein, J.A.; Dreyer, G.B. Total synthesis of (\pm)-calanolide A, a non-nucleoside inhibitor of HIV-1 reverse transcriptase. *J. Org. Chem.* **1993**, *58*, 5605–5606. [[CrossRef](#)]
15. Liu, J.; Li, Z.; Tong, P.; Xie, Z.; Zhang, Y.; Li, Y. TMSI-Promoted Vinylogous Michael Addition of Siloxyfuran to 2-Substituted Chromones: A General Approach for the Total Synthesis of Chromanone Lactone Natural Products. *J. Org. Chem.* **2015**, *80*, 1632–1643. [[CrossRef](#)] [[PubMed](#)]
16. Cortés, I.; Cordisco, E.; Kaufman, T.S.; Sortino, M.A.; Svetaz, L.A.; Bracca, A.B.J. First total synthesis of chromanone A, preparation of related compounds and evaluation of their antifungal activity against *Candida albicans*, a biofilm forming agent. *RSC Adv.* **2021**, *11*, 19587–19597. [[CrossRef](#)]
17. Cortés, I.; Kaufman, T.S.; Bracca, A.B.J. Short and Efficient First Total Synthesis of the Natural Product Chromanone A, a Chromone Derivative from the Algicolous Marine Fungus *Penicillium* sp. *Chem. Proc.* **2020**, *1*, 8300. [[CrossRef](#)]
18. Lee, H.; Yuan, Y.; Rhee, I.; Corson, T.W.; Seo, S.-Y. Synthesis of Natural Homoisoflavonoids Having Either 5,7-Dihydroxy-6-methoxy or 7-Hydroxy-5,6-dimethoxy Groups. *Molecules* **2016**, *21*, 1058. [[CrossRef](#)]
19. Kerste, E.; Harms, K.; Koert, U. Total Synthesis of (–)-Preussochromone D. *Org. Lett.* **2019**, *21*, 4374–4377. [[CrossRef](#)]
20. Emami, S.; Ghanbarimasir, Z. Recent advances of chroman-4-one derivatives: Synthetic approaches and bioactivities. *Eur. J. Med. Chem.* **2015**, *93*, 539–563. [[CrossRef](#)]
21. Keri, R.S.; Budagumpi, S.; Pai, R.K.; Balakrishna, R.G. Chromones as a privileged scaffold in drug discovery: A review. *Eur. J. Med. Chem.* **2014**, *8*, 340–374. [[CrossRef](#)]
22. Kamboj, S.; Singh, R. Chromanone-A Prerogative Therapeutic Scaffold: An Overview. *Arab. J. Sci. Eng.* **2021**, 1–37. [[CrossRef](#)]
23. Santos, C.M.M.; Silva, A.M.S. Six-membered ring systems: With O and/or S atoms. *Prog. Heterocycl. Chem.* **2021**, *32*, 501–563. [[CrossRef](#)]
24. Chitti, S.; Pulya, S.; Nandikolla, A.; Patel, T.K.; Kumar, B.K.; Murugesan, S.; Ghosh, B.; Sekhar, K.V.G.C. Design, synthesis and biological evaluation of 7-(5-((substituted-amino)-methyl)-thiophen-2-yl)-spiro-[chroman-2,4'-piperidin]-4-one hydrochloride analogues as anticancer agents. *Bioorg. Chem.* **2021**, *112*, 104865. [[CrossRef](#)] [[PubMed](#)]
25. Chen, H.; Xie, J.; Xing, D.; Wang, J.; Tang, J.; Yi, Z.; Xia, F.; Qiu, W.-W.; Yang, F. Diastereoselective synthesis of 3,3-disubstituted 3-nitro-4-chromanone derivatives as potential antitumor agents. *Org. Biomol. Chem.* **2019**, *17*, 1062–1066. [[CrossRef](#)]
26. Yurttas, L.; Temel, H.E.; Aksoy, M.O.; Bülbül, E.F.; Çiftçi, G.A. New chromanone derivatives containing thiazoles: Synthesis and antitumor activity evaluation on A549 lung cancer cell line. *Drug Dev. Res.* **2021**, 1–15. [[CrossRef](#)]
27. Tuong, T.L.; Do, L.T.M.; Aree, T.; Wonganan, P.; Chavasiri, W. Tetrahydroxanthone-chromanone heterodimers from lichen *Usnea aciculifera* and their cytotoxic activity against human cancer cell lines. *Fitoterapia* **2020**, *147*, 104732. [[CrossRef](#)]
28. Yu, G.Y.; Xiao, T. Recent advances in the research of chromone and thiochromone derivatives as antifungal agents. *Chin. J. Antibiot.* **2011**, *36*, 481–486.
29. Elghareeb, F.H.; Kandil, E.M.; Abou-Elzahab, M.; Abdelmoteleb, M.; Abozeid, M.A. Rigid 3D-spiro chromanone as a crux for efficient antimicrobial agents: Synthesis, biological and computational evaluation. *RSC Adv.* **2021**, *11*, 21301–21314. [[CrossRef](#)]
30. Yu, J.S.; Li, C.; Kwon, M.; Oh, T.; Lee, T.H.; Kim, D.H.; Ahn, J.S.; Ko, S.-K.; Kim, C.S.; Cao, S.; et al. Herqueilenone A, a unique rearranged benzoquinone-chromanone from the Hawaiian volcanic soil-associated fungal strain *Penicillium herquei* FT729. *Bioorg. Chem.* **2020**, *105*, 104397. [[CrossRef](#)]
31. Prakash, O.; Kumar, R.; Sehrawa, R. Synthesis and antibacterial activity of some new 2,3-dimethoxy-3-hydroxy-2-(1-phenyl-3-aryl-4-pyrazolyl)chromanones. *Eur. J. Med. Chem.* **2009**, *44*, 1763–1767. [[CrossRef](#)]
32. Ma, J.; Cao, B.; Chen, X.; Xu, M.; Bi, X.; Guan, P.; Jiang, Y.; Xu, J.; Han, L.; Huang, X. Violacin A, a new chromanone produced by *Streptomyces violaceoruber* and its anti-inflammatory activity. *Bioorg. Med. Chem. Lett.* **2018**, *28*, 947–951. [[CrossRef](#)] [[PubMed](#)]
33. Castro, H.; Cruz, T.; Amaral, P.A.; Cardoso, P.S.; Alsaffar, A.; Farrell, P.; Tomás, A.M.; Barlow, J.W. Synthesis and evaluation of novel chromanone and quinolinone analogues of uniflorol as anti leishmanial agents. *Heliyon* **2020**, *6*, e03614. [[CrossRef](#)] [[PubMed](#)]
34. Sneha, E.; Jessica, J.; Philip, E.; Shanty, A.A.; Kurup, M.R.P.; Mohanan, P.V. Novel class of mononuclear 2-methoxy-4-chromanones ligated Cu (II), Zn (II), Ni (II) complexes: Synthesis, characterisation and biological studies. *Inorg. Chim. Acta* **2018**, *478*, 155–165. [[CrossRef](#)]
35. Park, J.; Park, J.-E.; Seo, Y.-W.; Han, J.-S. 5,7-Dimethoxy-3-(2'-hydroxybenzyl)-4-chromanone inhibits α -glucosidase in vitro and alleviates postprandial hyperglycemia in diabetic mice. *Eur. J. Pharmacol.* **2019**, *863*, 172683. [[CrossRef](#)]
36. Gupta, O.; Pradhan, T.; Bhatia, R.; Monga, V. Recent advancements in anti-leishmanial research: Synthetic strategies and structural activity relationships. *Eur. J. Med. Chem.* **2021**, *223*, 113606. [[CrossRef](#)] [[PubMed](#)]
37. Coll, S.; Alhazmi, M.; Amaral, P.A.; Delmas, S.B.; Lamer, A.-C.L.; Barlow, J.W. Synthesis and Evaluation of Novel 2,2-Dimethylthiochromanones as Anti-Leishmanial Agents. *Molecules* **2021**, *26*, 2209. [[CrossRef](#)] [[PubMed](#)]

38. Zhao, P.-L.; Li, J.; Yang, G.-F. Synthesis and insecticidal activity of chromanone and chromone analogues of diacylhydrazines. *Bioorg. Med. Chem.* **2007**, *15*, 1888–1895. [[CrossRef](#)] [[PubMed](#)]
39. Xiao, L.; Yu, L.; Li, P.; Chi, J.; Tang, Z.; Li, J.; Tan, S.; Wang, X. Design, Synthesis, and Bioactivity Evaluation of New Thiochromanone Derivatives Containing a Carboxamide Moiety. *Molecules* **2021**, *26*, 4391. [[CrossRef](#)]
40. Yu, L.; Chi, J.; Xiao, L.; Li, J.; Tang, Z.; Tan, S.; Li, P. Novel Thiochromanone Derivatives Containing a Sulfonyl Hydrazone Moiety: Design, Synthesis, and Bioactivity Evaluation. *Molecules* **2021**, *26*, 2925. [[CrossRef](#)] [[PubMed](#)]
41. Yu, L.; Xiao, L.; Chi, J.; Tang, Z.; Li, J.; Tan, S.; Li, P. Design, synthesis, and bioactivity evaluation of novel thiochromanone derivatives containing an oxime or oxime ether moiety. *J. Heterocycl. Chem.* **2021**, *58*, 2124–2131. [[CrossRef](#)]
42. Collado, I.G.; Aleu, J. Metabolism of Antifungal Thiochroman-4-ones by *Trichoderma viride* and *Botrytis cinerea* Cristina Pinedo-Rivilla. *J. Nat. Prod.* **2018**, *81*, 1036–1040. [[CrossRef](#)]
43. Gnanasekaran, K.K.; Benbrook, D.M.; Nammalwar, B.; Thavathiru, E.; Bunce, R.A.; Berlin, K.D. Synthesis and evaluation of second generation Flex-Het scaffolds against the human ovarian cancer A2780 cell line. *Eur. J. Med. Chem.* **2015**, *96*, 209–217. [[CrossRef](#)] [[PubMed](#)]
44. Demirayak, S.; Yurttas, L.; Karaburun, N.G.; Karaburun, A.C.; Kayagil, I. New chroman-4-one/thiochroman-4-one derivatives as potential anticancer agents. *Saudi Pharm. J.* **2017**, *25*, 1063–1072. [[CrossRef](#)] [[PubMed](#)]
45. Hammam, A.E.-F.G.; Fahmy, A.F.M.; Amr, A.-G.E.; Mohamed, A.M. Synthesis of novel tricyclic heterocyclic compounds as potential anticancer agents using chromanone and thiochromanone as synthons. *Indian J. Chem. Sect. B* **2003**, *42*, 1985–1993. [[CrossRef](#)]
46. Song, J.; Pan, R.; Li, G.; Su, W.; Song, X.; Li, J.; Liu, S. Synthesis and anticancer activities of thiosemicarbazones derivatives of thiochromanones and related scaffolds. *Med. Chem. Res.* **2020**, *29*, 630–642. [[CrossRef](#)]
47. Nussbaumer, P.; Lehr, P.; Billich, A. 2-Substituted 4-(Thio)chromenone 6-O-Sulfamates: Potent Inhibitors of Human Steroid Sulfatase. *J. Med. Chem.* **2002**, *45*, 4310–4320. [[CrossRef](#)] [[PubMed](#)]
48. Smith, H.J.; Nicholls, P.J.; Simons, C.; Lain, R.L. Inhibitors of steroidogenesis as agents for the treatment of hormone-dependent cancers. *Expert Opin. Ther. Pat.* **2001**, *11*, 789–824. [[CrossRef](#)]
49. Zimmer, L.; Fournet, G.; Joseph, B.; Guillaumet, G.; Bars, D.L. Carbon-11 labelling of 8-[[3-[4-(2-[¹¹C]methoxyphenyl)piperazin-1-yl]-2-hydroxypropyl]oxy]thiochroman, a presynaptic 5-HT_{1A} receptor agonist, and its in vivo evaluation in anaesthetised rat and in awake cat. *Nucl. Med. Biol.* **2003**, *30*, 541–546. [[CrossRef](#)]
50. Zhang, D.; Ji, X.; Gao, R.; Wang, H.; Meng, S.; Zhong, Z.; Li, Y.; Jiang, J.; Li, Z. Synthesis and antiviral activities of a novel class of thioflavone and flavonoid analogues. *Acta Pharm. Sin. B* **2012**, *2*, 575–580. [[CrossRef](#)]
51. Steiner, G.; Schmidt, T.; Kordes, M.; von Deyn, W.; Hofmann, M.; Baumann, E.; Puhl, M.; Heffernan, G.; Culbertson, D.L.; Treacy, M.F. Amino-Substituted Benzo(Hetero)Cyclic Derivatives, Particularly 1-Alkyl-4-Benzo(Hetero)Cyclicsubstituted Piperazines, Useful as Insecticides, Acaricides, and Nematocides, and Their Preparation, Uses, and Compositions. PCT International Application WO 2004080170, 23 September 2004.
52. Subramaniyan, G.; Jayashankaran, J.; Raghunathan, R. Novel Synthesis of N-Methyl Spiropyrrolidines by 1,3-Dipolar Cycloaddition Reaction of Azomethine Ylides. *Synth. Commun.* **2006**, *35*, 2189–2193. [[CrossRef](#)]
53. Rani, G.U.; Kumar, S.V.; Bharkavi, C.; Menéndez, J.C.; Perumal, S. One-Pot Access to a Library of Dispiro Oxindole-pyrrolidine/pyrrolothiazole-thiochromane Hybrids via Three-Component 1,3-Dipolar Cycloaddition Reactions. *ACS Comb. Sci.* **2016**, *18*, 337–342. [[CrossRef](#)]
54. Haddad, S.; Boudriga, S.; Porzio, F.; Soldera, A.; Askri, M.; Sriram, D.; Yogeewari, P.; Knorr, M.; Rousselin, Y.; Kubicki, M.M. Synthesis of Novel Dispiropyrrrolothiazoles by Three-Component 1,3-Cipolar Cycloaddition and Evaluation of Their Antimycobacterial Activity. *RSC Adv.* **2014**, *4*, 59462–59471. [[CrossRef](#)]
55. Haddad, S.; Boudriga, S.; Akhaja, T.N.; Raval, J.P.; Porzio, F.; Soldera, A.; Askri, M.; Knorr, M.; Rousselin, Y.; Kubicki, M.M.; et al. A Strategic Approach to the Synthesis of Functionalized Spirooxindole Pyrrolidine Derivatives: In vitro Antibacterial, Antifungal, Antimalarial and Antitubercular studies. *New J. Chem.* **2015**, *39*, 520–528. [[CrossRef](#)]
56. Mhiri, C.; Boudriga, S.; Askri, M.; Knorr, M.; Sriram, D.; Yogeewari, P.; Nana, F.; Golz, C.; Strohmanni, C. Design of Novel Dispirooxindolopyrrolidine and Dispirooxindolopyrrolothiazole Derivatives as Potential Antitubercular Agents. *Bioorg. Med. Chem. Lett.* **2015**, *25*, 4308–4313. [[CrossRef](#)] [[PubMed](#)]
57. Toumi, A.; Boudriga, S.; Hamden, K.; Daoud, I.; Askri, M.; Soldera, A.; Lohier, J.-F.; Strohmanni, C.; Brieger, L.; Knorr, M. Diversity-Oriented Synthesis of Spiropyrrrolo[1,2-a]isoquinoline Derivatives via Diastereoselective and Regiodivergent Three-Component 1,3-Dipolar Cycloaddition Reactions: In Vitro and in Vivo Evaluation of the Antidiabetic Activity of Rhodanine Analogues. *Org. Chem.* **2021**, *86*, 13420–13445. [[CrossRef](#)]
58. Chai, J.D.; Head-Gordon, M. Long-Range Corrected Hybrid Density Functionals with Damped Atom-Atom Dispersion Corrections. *Phys. Chem. Chem. Phys.* **2008**, *10*, 6615–6620. [[CrossRef](#)]
59. Barone, V.; Cossi, M. Quantum calculation of molecular energies and energy gradients in solution by a conductor solvent model. *J. Phys. Chem. A* **1998**, *102*, 1995–2001. [[CrossRef](#)]
60. Cossi, M.; Scalmani, G.; Rega, N.; Barone, V. New developments in the polarizable continuum model for quantum mechanical and classical calculations on molecules in solution. *J. Chem. Phys.* **2002**, *117*, 43–54. [[CrossRef](#)]
61. Rattan, A. *Antimicrobials in Laboratory Medicine*; B.I. Churchill Livingstone: New Delhi, India, 2000; Volume 85, p. 108.

62. Asad, M.; Arshad, M.N.; Asiri, A.M.; Khan, S.A.; Rehan, M.; Oves, M. Synthesis, Characterization, Molecular Docking and Antimicrobial Activity of Novel Spiropyrrolidine Derivatives. *Polycycl. Aromat. Compd.* **2021**. [[CrossRef](#)]
63. Hassaneen, H.M.E.; Eid, E.M.; Eid, H.A.; Farghaly, T.A.; Mabkhot, Y.N. Facial Regioselective Synthesis of Novel Bioactive Spiropyrrolidine/Pyrrolizine-Oxindole Derivatives via a Three Components Reaction as Potential Antimicrobial Agents. *Molecules* **2017**, *22*, 357. [[CrossRef](#)] [[PubMed](#)]
64. Frisch, M.J.; Trucks, G.W.; Schlegel, H.B.; Scuseria, G.E.; Robb, M.A.; Cheeseman, J.R.; Scalmani, G.; Barone, V.; Petersson, G.A.; Nakatsuji, H. *Gaussian 16, Revision B.01*; Gaussian, Inc.: Wallingford, CT, USA, 2016.
65. Miar, M.; Shiroudi, A.; Pourshamsian, K.; Olliaey, A.R.; Hatamjafari, F. Theoretical investigations on the HOMO–LUMO gap and global reactivity descriptor studies, natural bond orbital, and nucleus-independent chemical shifts analyses of 3-phenylbenzo[d]thiazole-2(3H)-imine and its para-substituted derivatives: Solvent and substituent effects. *J. Chem. Res.* **2020**, *45*, 147–158. [[CrossRef](#)]
66. Pearson, R.G. Hard and Soft Acids and Bases. *J. Am. Chem. Soc.* **1963**, *85*, 3533–3539. [[CrossRef](#)]
67. Erol, M.; Celika, I.; Kuyucuklu, G. Synthesis, Molecular Docking, Molecular Dynamics, DFT and Antimicrobial Activity Studies of 5-substituted-2-(p-methylphenyl)benzoxazole Derivatives. *J. Mol. Struct.* **2021**, *1234*, 130151. [[CrossRef](#)]
68. Pearson, R.G. Chemical hardness and the electronic chemical potential. *Inorg. Chim. Acta* **1992**, *198–200*, 781–786. [[CrossRef](#)]
69. Pearson, R.G. Maximum Chemical and Physical Hardness. *J. Chem. Ed.* **1999**, *76*, 267–275. [[CrossRef](#)]
70. Islam, N.; Ghosh, D.C. On the Electrophilic Character of Molecules Through Its Relation with Electronegativity and Chemical Hardness. *Int. J. Mol. Sci.* **2012**, *13*, 2160. [[CrossRef](#)] [[PubMed](#)]
71. Bhat, A.R.; Dongre, R.S.; Almalki, F.A.; Berredjem, M.; Aissaoui, M.; Touzani, R.; Ben Hadda, T.; Akhter, M.S. Synthesis, biological activity and POM/DFT/docking analyses of annulated pyrano[2,3-d]pyrimidine derivatives: Identification of antibacterial and antitumor pharmacophore sites. *Bioorg. Chem.* **2021**, *106*, 104480. [[CrossRef](#)]
72. Ghareeb, E.A.; Mahmoud, N.F.H.; El-Bordany, E.A.; El-Helw, E.A.E. Synthesis, DFT, and eco-friendly insecticidal activity of some N-heterocycles derived from 4-((2-oxo-1,2-dihydroquinolin-3-yl)methylene)-2-phenyloxazol-5(4H)-one. *Bioorg. Chem.* **2021**, *112*, 104945. [[CrossRef](#)]
73. Uzun, S.; Esen, Z.; Koç, E.; Usta, N.C.; Ceylan, M. Experimental and density functional theory (MEP, FMO, NLO, Fukui functions) and antibacterial activity studies on 2-amino-4-(4-nitrophenyl)-5,6-dihydrobenzo [h] quinoline-3-carbonitrile. *J. Mol. Struct.* **2019**, *1178*, 450–457. [[CrossRef](#)]
74. Lipinski, C.A. Lead- and drug-like compounds: The rule-of-five revolution. *Drug Discov. Today Technol.* **2004**, *1*, 337–341. [[CrossRef](#)] [[PubMed](#)]
75. Veber, D.F.; Johnson, S.R.; Cheng, H.Y.; Smith, B.R.; Ward, K.W.; Kopple, K.D. Molecular properties that influence the oral bioavailability of drug candidates. *J. Med. Chem.* **2002**, *45*, 2615–2623. [[CrossRef](#)] [[PubMed](#)]
76. Dolomanov, O.V.; Bourhis, L.J.; Gildea, R.J.; Howard, J.A.K.; Puschmann, H. OLEX2: A complete structure solution, refinement and analysis program. *J. Appl. Crystallogr.* **2009**, *42*, 339–341. [[CrossRef](#)]
77. Sheldrick, G.M. SHELXT—Integrated space-group and crystal-structure determination. *Acta Crystallogr. A* **2015**, *71*, 3–8. [[CrossRef](#)] [[PubMed](#)]
78. Sheldrick, G.M. Crystal structure refinement with SHELXL. *Acta Cryst. C71* **2015**, *C71*, 3–8. [[CrossRef](#)]
79. Dennington, R.; Keith, T.A.; Millam, J.M. *GaussView, Version 6.0.16*; Semichem Inc.: Shawnee Mission, KS, USA, 2016.
80. Pérez, P.; Domingo, L.R.; Aurell, M.J.; Contreras, R. Quantitative characterization of the global electrophilicity pattern of some reagents involved in 1,3-dipolar cycloaddition reactions. *Tetrahedron* **2003**, *59*, 3117–3125. [[CrossRef](#)]
81. Parr, R.G.; Szentpaly, L.; Liu, S. Electrophilicity Index. *J. Am. Chem. Soc.* **1999**, *121*, 1922–1924. [[CrossRef](#)]
82. Fukui, K. Role of frontier orbitals in chemical reactions. *Science* **1982**, *21*, 747–754. [[CrossRef](#)]